

ABSTRACT

KAMATH, AJITH M. Asymptotic Analysis of Large Antenna Arrays for Communications and Radar Applications. (Under the direction of Prof. Brian L. Hughes.)

In recent years there has been a growing interest in using antenna arrays at both ends of a wireless communication link. Such multiple input multiple output (MIMO) systems are beneficial both in terms of providing greatly improved data rates, as well as in terms of robustness in combating errors compared to systems which use only one antenna. These benefits are obtained without requiring extra transmit power or spectral bandwidth, but come at the cost of additional processing power. In radar, multiple antenna arrays have been in use for several decades. Even so, the idea of measuring the full received electro-magnetic (EM) wave for parameter estimation has been a recent one. In this dissertation, we address two issues through asymptotics: in MIMO systems, we develop insights into finite MIMO array performance by deriving precise results for asymptotically large MIMO arrays, and in radar we derive the gain from measuring the complete field over a spherical surface versus measuring only one polarization component using an equal number of sensors.

First, we consider the distribution of the mutual information of a MIMO system with an uncorrelated Rayleigh fading channel. We show that, as the transmit and receive array sizes tend to infinity while maintaining their ratio constant, the mutual information distribution tends to Gaussian distribution at all signal to noise ratios (SNRs), and give a closed-form expression for its mean and variance. Through simulations, we observe that the mutual information distribution of a finite MIMO system with as few as 4 array elements at either end has a variance which depends only on the ratio of the two arrays and is also closely approximated by the asymptotic distribution variance. We show that the mean of the distribution can also be approximated much closer than previously shown, and hence combined with the asymptotic variance, this yields close approximations for outage capacities.

We next consider the problem of determining the best possible tradeoff between diversity and multiplexing gains in an uncorrelated Rayleigh fading channel. Zheng and Tse have characterized this tradeoff in the large signal to noise ratio(SNR) limit.

We apply our asymptotic results on mutual information to compute the finite SNR diversity-multiplexing tradeoffs at high outage probabilities in the range of practical interest. We show that the asymptotic results match the tradeoffs derived by Zheng and Tse only in the equal antenna MIMO array case. We then propose a linear dispersion coding scheme which modulates a block of data by picking a random unitary matrix, which was previously shown to produce full-rank full-diversity code-books with probability one. Through simulations using rectangular code-books, we show that these may also achieve the full Zheng-Tse diversity multiplexing tradeoff after using a maximum likelihood (ML) decoder.

Having developed fundamental insights into MIMO arrays through the use of asymptotic analysis, we consider the impact of using vector antennas in large radar arrays. Specifically, we compare the performance of range and direction-of-arrival (DOA) estimation of a single source using an array of vector electro-magnetic (EM) sensors packed densely on the surface of a sphere, with a similarly shaped array with identically oriented dipole elements. We compute the Cramer-Rao lower bound on maximum-likelihood range and DOA estimation using either array. By taking the ratio of the confidence volumes as the gain, we compare the vector array estimate with the uni-polarized array as a function of target location.

**Asymptotic Analysis of Large Antenna Arrays for Communications and
Radar Applications**

by

Ajith M. Kamath

A dissertation submitted to the Graduate Faculty of
North Carolina State University
in partial fulfillment of the
requirements for the Degree of
Doctor of Philosophy

Electrical Engineering

Raleigh, NC

2005

Approved By:

Dr. Hamid Krim

Dr. Jack W. Silverstein

Dr. Brian L. Hughes
Chair of Advisory Committee

Dr. Alexandra Duel-Hallen

Biography

Ajith M. Kamath is from Bangalore, India. He received his undergraduate education from the Indian Institute of Technology, Chennai (IIT-M, Chennai was formerly called Madras) starting from August 1996 to June 2000. He commenced his graduate studies at NCSU in August 2000 and defended his PhD in December 2005. During his PhD, he worked as a research assistant under the supervision of his advisor, Dr. Brian L. Hughes, with funding from the National Science Foundation (NSF). He is interested in information theory, signal processing algorithms, coding theory and their applications in wireless communications.

Earlier, he was ranked first in the Indian National Math Olympiad in the year 1995. He was a recipient of the National Board for Higher Mathematics (NBHM, India) scholarship, for four successive academic years from 1997 to 2000.

To my parents and sister

Acknowledgements

I would like to express my sincere gratitude to my advisor, Dr. Brian Hughes, for his support and guidance throughout my study at NC State. Dr. Hughes' expert knowledge and insightful ideas are a source of inspiration for his students. I used to meet Dr. Hughes almost every week for a good long hour during which we freely explored new avenues for advancement. Dr. Hughes always appreciated my ideas unassumingly and only offered constructive criticism. My discussions with Dr. Hughes also improved my critical thinking skills. I am thankful for his conducting weekly seminars and inviting guest speakers, all of which which gave me some depth of knowledge and got me up to speed early during my PhD. Dr. Hughes is also one of the most effective teachers I've met in a classroom.

Having studied at NCSU, I have also been extremely fortunate to have had access to Dr. Jack Silverstein, who is a much sought after expert in random matrix theory and whose papers are widely cited in the information theory literature. His theorems indeed lie at the foundation of this dissertation, and provide legitimacy to its results. I would like to thank him for his readiness to discuss ideas and tackle problems that were beyond my area of expertise. I would also like to thank Dr. Alexandra Duel-Hallen and Dr. Hamid Krim for serving on my committee. Taking their courses early in my graduate studies proved to be very helpful.

I would like to appreciate the excellent library facilities at NCSU, which made finding books and references extremely easy. I would also like to acknowledge the search phenomenon that is Google. In particular, I should mention Google Scholar, which combined with the university library access to journal papers, are sure to be an unbeatable combination for research. My knowledge of my subject significantly expanded after I started using Google Scholar, especially because of its citations feature which helps in tracking the entire tree of ideas.

One cannot underestimate the importance of a peer group in an emotionally taxing endeavor such as a PhD. I am grateful for the company of my colleagues Pallav Sudarshan, Sandeep Krishnamurthy, Chris Mary James, Xinying Yu, and Mahmud Al Naser, all whom I've known for the longest period of time. It was particularly a

pleasure, and also an inspiration, to collaborate with Pallav and Sandeep in research. I have also had stimulating discussions with students in Dr. Gianluca Lazzi's group, namely, Keyoor Gosalia, Anand Konanur, Ajit Rajagopal, and Gaurav Gupta. I thank Nishant Jacob, Carmela Cozzo and Zhihong Hong, for their help and advice early in my PhD.

My greatest debt is to my parents and sister for their unconditional love and support, which got me so far. My parents encouragement and faith in me have truly kept me on track and ensured my progress. I am grateful to my sister Ashwini for keeping my spirits up with her stories and emails.

Finally, I thank all my friends here at NCSU and elsewhere, for greatly enriching my life outside my graduate studies.

Contents

List of Figures	viii
1 Introduction	1
1.1 The Wireless Channel	2
1.2 Multiple-Antenna Communications	4
1.3 Space-Time Coding	7
1.4 Applications of Antenna Arrays in Radar	9
1.5 Dissertation Overview	10
2 The Asymptotic Capacity of Multiple-Antenna Rayleigh Fading Channels	14
2.1 Random Matrix Theory	16
2.2 Asymptotic Capacity Distribution	18
2.3 Numerical Results	23
2.4 Conclusions	24
3 On the Diversity Multiplexing Tradeoff of Large MIMO Arrays	32
3.1 Large Array Tradeoffs	34
3.2 Achieving the Diversity-Multiplexing Tradeoff	43
3.3 Conclusions	50
4 Impact of Vector Antennas on Range and Direction Estimation Using a Spherical Array	51
4.1 Problem Formulation	53
4.2 Cramer-Rao Bounds	56
4.2.1 Tri-polarized Spherical Array	57
4.2.2 Uni-polarized Spherical Array	60
4.3 Gain From Polarization	61
4.4 Conclusions	65

5	Conclusions	67
	Bibliography	69
A	Asymptotic Variance Derivation	77
B	Asymptotic Variance and Stieltjes Transform	80

List of Figures

1.1	Representation of a MIMO channel	5
1.2	The basic principle of radar.	9
2.1	Ergodic capacity for $t \times r = 1 \times 1, 2 \times 2, 4 \times 4, 8 \times 8$ and 16×16	25
2.2	10% outage rate for $t \times r = 1 \times 1, 2 \times 2, 4 \times 4, 8 \times 8$ and 16×16	26
2.3	1% outage rate for $t \times r = 1 \times 1, 2 \times 2, 4 \times 4, 8 \times 8$ and 16×16	26
2.4	Ergodic capacity for $t \times r = 2 \times 1, 4 \times 2, 6 \times 3$ and 8×4	27
2.5	10% outage rate for $t \times r = 2 \times 1, 4 \times 2, 6 \times 3$ and 8×4	27
2.6	1% outage rate for $t \times r = 2 \times 1, 4 \times 2, 6 \times 3$ and 8×4	28
2.7	Ergodic capacity for $t \times r = 4 \times 1, 8 \times 2, 12 \times 3$ and 16×4	28
2.8	10% outage rate for $t \times r = 4 \times 1, 8 \times 2, 12 \times 3$ and 16×4	29
2.9	1% outage rate for $t \times r = 4 \times 1, 8 \times 2, 12 \times 3$ and 16×4	29
2.10	Standard deviation of the mutual information for equal antenna MIMO systems.	30
2.11	Standard deviation of the mutual information for increasing $c = r/t$, starting from $c = 4/24 = 1/6, 1/3, 1/2, 2/3$ to $24/24 = 1$	31
3.1	The Zheng-Tse diversity multiplexing tradeoff curve.	36
3.2	Asymptotic empirical eigenvalue distribution(EED) of a $r \times t$ matrix $\frac{1}{t}HH^\dagger$ for two cases, $r = t$ and $2r = t$, as $r, t \rightarrow \infty$	40
3.3	Large array asymptotic diversity multiplexing tradeoff curves for fixed SNRs starting from 0dB to 40dB, in steps of 5dB, for equal antenna MIMO arrays compared with the 4×4 MIMO system Zheng-Tse tradeoff.	42
3.4	Large array asymptotic diversity multiplexing tradeoff curves for fixed SNRs starting from -5 dB to 25 dB, in steps of 5dB, for unequal antenna MIMO arrays $r/t = c = 1/2$	43
3.5	Actual outage probability curves for a 4×4 MIMO system obtained experimentally versus the curves predicted by the asymptotic formula (3.6) for an increasing sequence of rates $R = 4, 8, \dots, 20$	44

3.6	Actual outage probability curves for a 8×4 MIMO system obtained experimentally versus the curves predicted by the asymptotic formula (3.6) for an increasing sequence of rates $R = 4, 8, \dots, 20$	45
3.7	Block error rate(BER) with ML decoding(using a sphere decoder) for successive constellations with rates $R = 4, 8, 12, 16, 20$, alongside the corresponding outage probability curves.	48
3.8	Probability density function(PDF) of the unordered eigenvalue λ of $\frac{1}{2}DD^*$ (where $D = X_i - X_j$ is the codeword difference matrix) for the Yao-Wornell codebook [61]. For the codebook obtained by unitary dispersion of the 64-QAM constellation, the eigenvalue λ corresponding to $\frac{1}{3}DD^*$ is plotted(the fraction $\frac{1}{3}$ normalises the power in each row to 1, in accordance with Silverstein's limiting distribution theorem [42]). In both cases, the PDF is approximated by plotting the 100-bin histogram of 10^5 randomly generated 2×3 codeword matrices.	49
4.1	Spherical co-ordinate system with radius r , elevation angle θ and azimuth ϕ	54
4.2	Spherical array with infinitesimal tripole antennas distributed uniformly on its surface, receiving a dual-polarized plane wave from a direction of arrival $\{\theta, \phi\}$	58
4.3	Ratio of confidence ellipsoid volume versus elevation angle, between an array of tri-polarized antennas and a uni-polarized antenna array. Both the arrays have a wavelength-normalized radius of $R = 10$, and the incoming wave is circularly polarized. The ticks on the x-axis mark the normalized elevation angle $(\frac{\theta}{\pi})$, for θ in the range $\frac{\pi}{5} < \theta < \frac{\pi}{2}$	66

Chapter 1

Introduction

The civilian use of wireless communications in the form of cellular telephony can be regarded as having started in Finland in 1971. The ARP (Autoradiopuhelin, Car Radio Phone in English) was the first commercially-operated public mobile phone network, but the equipment was bulky and occupied a significant portion of a car trunk. In 1983, the first fully-mobile cellphones based on the analog standard called AMPS (Advanced Mobile Phone System) were deployed in Chicago. With the advent of digital standards such as D-AMPS and GSM in the late 80s to early 90s, mobile phones became easier to carry around, and the coverage also became more widespread. This was also made possible in large part by parallel advances in hardware technologies. Since then, the pace of change has been rapid, which has led to a proliferation of mobile phones based on new standards such as IS-95, CDMA2000, EDGE and UMTS. Today mobile phones have moved beyond mere voice telephony towards a variety of data services, such as text messaging, email, photography, video, TV, email, internet browsing, and GPS-based navigation services. All these applications have increased the demand for higher data rates.

The theoretical foundations of digital telephony were laid by Claude Shannon as

early as the 1940's in his landmark paper, "The mathematical theory of communication" [40]. In this paper he described a complete methodology by which one could compute the ultimate limit to error-free communication over any channel corrupted by noise, which he called the capacity of the channel. It took several decades before practical schemes were invented which could approach this theoretical limit even on the simplest examples of channels.

In practice, communicating close to the optimum performance guaranteed by theory requires considerable processing power, and this in turn also limits the performance. Hence, sub-optimal algorithms are used which require computations several orders of magnitude less than the optimal algorithms and yet achieve a significant fraction of the optimal performance. Thanks to extremely rapid advances in VLSI chip integration and increases in processing power as described by Moore's law, the feasibility of packing more than one antenna at the mobile handset has been considered in the past decade, starting in the mid 1990s. This has produced a great wealth of literature regarding the optimal performance of wireless links employing multiple-antenna arrays (often referred to as multiple input multiple output systems, or MIMO for short) under a variety of conditions and both optimal and sub-optimal computationally efficient schemes for achieving performance close to the limits.

1.1 The Wireless Channel

Unlike wire-line media such as copper wire or optic fibres in which the transmission medium is fixed, communication using electromagnetic(EM) radiation propagating through free space is subject to a variety of random influences which make the engineering challenges all the more interesting. The environment reflects, refracts, and delays the EM waves as they travel between the transmitter and receiver where it is

further corrupted by thermal noise. The signal is also attenuated significantly due to an inverse fourth or greater power of distance propagation loss. When multiple users share a channel, their signals may interfere with each other. The goal of a wireless system designer is to combat all these losses by devising appropriate transmission and signal processing strategies at the receiver to recover the data within a given quality of service guarantee. Furthermore, these strategies have to be devised constrained by the limited resources such as bandwidth, the limited energy stored in a battery and limitations on radiated power as fixed by the Federal Communications Commission (FCC).

Until about a decade ago, the random effects of the environment on the transmitted signal were considered more as a nuisance to be combated than as a resource which could be exploited. In the early to mid 90's the pioneering ideas of Witneben [60], Foschini and Gans [10] and Telatar [46] suggested that multiple-antenna systems could utilize the environmental propagation effects in order to provide data rates that were hitherto unheard of, while incurring no extra cost in bandwidth or power. One of the key insights motivating this idea was the observation that in a sufficiently rich scattering environment, antennas separated by a distance greater than half the carrier signal wavelength are mutually uncorrelated. This fact could be exploited to cancel out interfering signals at each receiver antenna and create multiple parallel 'data pipes' between the transmitter and receiver.

These ideas were further crystallized when Telatar [46] published an information theoretic analysis of a simple multiple-antenna channel model, yet one which encompassed many of the effects of propagation. By deriving the capacity of a system with any given number of transmit and receive antennas, he demonstrated the gains that were possible over systems which used only a single antenna at each end.

1.2 Multiple-Antenna Communications

Now we shall explore Telatar's results in more detail since they are of great relevance to this thesis. We shall consider a point-to-point wireless link with t transmit antennas and r receive antennas. The data symbols output from the transmit array over n channel uses, can be represented as a $t \times n$ matrix X . The transmitted signals are assumed to be normalized to unit power, $(1/tn) \sum_{j=1}^t \sum_{l=1}^n |X_{jl}|^2 = 1$. The effect of the channel on the signal can be described by a linear transfer function, which can be represented as a $r \times t$ matrix H . The entries of H are all assumed to be independent and identically distributed (i.i.d. $\mathcal{CN}(0, 1)$) complex Gaussian random variables. This assumption can be justified by the fact that the signal at each receiver antenna is the superimposition of a large number of copies traveling through different paths combined with a random phase shift (see Fig 1.1). The receive array output samples over n channel uses, can then be represented as a $r \times n$ matrix Y . The receiver noise is assumed to be additive, white and complex Gaussian distributed (AWGN) (i.i.d. $\mathcal{CN}(0, 1)$) and is also represented as a $r \times n$ matrix N . The system equation may thus be written as

$$Y = \sqrt{\rho/t}HX + N.$$

where ρ represents the signal-to-noise ratio (SNR) per receive antenna.

We are interested in determining the maximum data throughput in such a system, as promised by information theory. The performance measures that are of interest to us vary depending on the prevailing channel conditions. In the block fading channel model, the channel transfer function changes several times over the duration of a single codeword. The reliability measure in such a case is called the ergodic capacity.

In an outage channel model, the channel stays fixed through the duration of a codeword. In this model, a bad channel severely constrains the amount the data we can transmit without error. In fact, there is no minimum data rate that can be

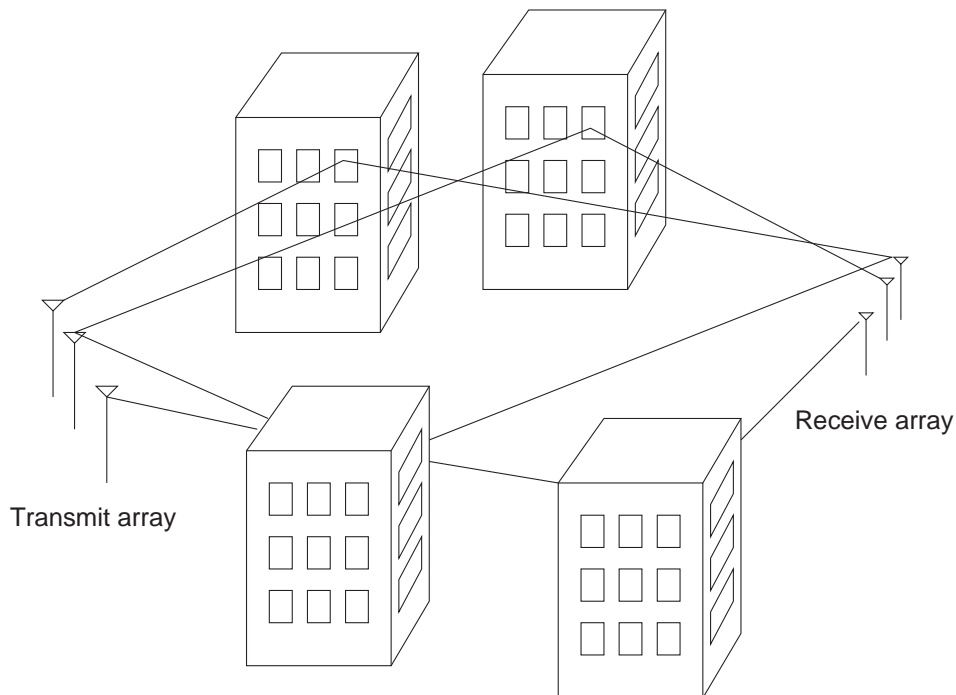


Figure 1.1: Representation of a MIMO channel

guaranteed over such a channel for all times. However, we can guarantee a minimum data rate when the user accepts a certain amount of outage time when the channel is bad and that transmitted data is lost. The minimum error free data rate that can be guaranteed when the channel is known to be good is called the outage capacity of the channel.

For the rest of this chapter, we assume that the channel matrix is perfectly known to the receiver. For a given channel realization h , the mutual information between the transmitted data and received samples is given by $I(Y, X|H = h) = \log \det(I + \rho/thh^*)$ [46] where ρ is the total signal to noise ratio (SNR) at the receiver and $(*)$ represents the conjugate-transpose of a matrix. The mutual information is a random variable that depends on the channel state H . In the ergodic channel case, the

channel capacity (called the ergodic capacity) is given by $E_h\{I(Y, X|H = h)\}$. In the outage channel scenario, the $P_{out}(R) = q\%$ outage rate is given by $C_q(t, r, \rho) = \sup\{R \geq 0 : \Pr[C(t, r, \rho) < R] \leq q\}$. It is the mutual information percentile point R below which the $q\%$ of channels are unable to support that data rate.

In the outage channel scenario, the performance gains with multiple antenna systems come from two sources. First, there is the multiplexing gain, which is given by the rank of the channel matrix H . It was shown by Telatar and others [10, 46], that in a $r \times t$ MIMO system, the maximum multiplexing gain that one can achieve is $\min(r, t)$. Second, there is the diversity gain which is defined precisely below. In a $r \times t$ system, the maximum diversity gain that can be obtained is rt . This can be easily achieved by transmitting the same data stream from all the transmit antennas.

The information-theoretic limits correspond to the case when we can code over infinite block-lengths of data. However, practical systems can code only over a finite block-length of data. Also, in any given transmission scheme, one can achieve either the maximum multiplexing gain or the maximum diversity gain, but not both simultaneously. Hence, it is of interest to characterize the exact tradeoffs between the multiplexing and diversity gains. For the large SNR regime, these issues were resolved to a great extent by Zheng and Tse [63] who gave the precise diversity and multiplexing tradeoffs in transmission schemes using finite block-lengths of code. Since the channel capacity increases linearly with $\log(SNR)$ at high SNRs, in order to achieve a certain fraction of the capacity at high SNR, we should consider schemes that support a data rate which also increases with SNR. Here, a scheme can be thought of as a family of codes of block length l , one at each SNR level. For example, a family of code-books of block length l over an increasing sequence of M-ary constellations forms a scheme. Let $R(SNR)$ (bits/symbol) be the rate of the code. Then the multiplexing

gain m is defined as

$$\lim_{SNR \rightarrow \infty} \frac{R(SNR)}{\log(SNR)} = m \quad (1.1)$$

and the diversity gain is defined in terms of outage error probability for the same rate $R(SNR)$ as

$$\lim_{SNR \rightarrow \infty} \frac{\log P_{out}(R(SNR))}{\log(SNR)} = -d \quad (1.2)$$

Then the precise tradeoffs for any scheme with code-books of block length $l \geq r+t-1$ are given as follows. Theorem: The optimal tradeoff curve is given by the piecewise-linear function connecting the points $(k, d^*(k))$, $k = 0, 1, \dots, \min\{r, t\}$ where

$$d^*(k) = (t - k)(r - k).$$

In particular, the maximum diversity gain $d_{max}^* = rt$ and the maximum multiplexing gain $m_{max}^* = \min(r, t)$.

1.3 Space-Time Coding

Shortly after the seminal information theoretic work of Telatar [46] and Foschini and Gans [10], several authors attempted to develop code designs that could achieve the performance gains promised by information theory. The general idea behind coding for diversity is that sending redundant information over a fading channel increases the probability that at least one of the copies is received correctly. In a MIMO fading channel, there are three kinds of diversity which correspond to the three kinds of fading observed on the channel: temporal, frequency and spatial fading. Channel fading over time and across frequencies also occurs in single-antenna based single input single output (SISO) systems. However, spatial fading across antennas is exclusive to MIMO systems, which requires new code designs to take advantage of this new source of diversity. Hence, codes designed for MIMO systems need to

introduce redundancy in the data across antennas in the transmit array in addition to the redundancy in time and across frequencies, which is why they are called space-time-frequency codes. In the narrowband MIMO channel, which is the focus of this dissertation, there is no frequency diversity, so the code designs in this case are called space-time codes.

One of the first practical schemes to demonstrate the large gains from using multiple-antenna systems was the V-BLAST scheme [11, 12, 15], which achieved the full multiplexing gain promised by theory. The design of space-time trellis codes was first considered in the ground-breaking paper by Tarokh, Seshadri and Calderbank [44], which gave the criteria for practical space-time code design. For outage channels the design criteria seek to maximize the rank and the determinant of codeword difference matrices. In the case of ergodic channels, one can use an interleaver to convert the channel into one varying from symbol to symbol. In this case, the design criteria for code design seek to maximize the Hamming distance and product distance of codeword difference matrices.

An alternative approach to code design was proposed in [16]. In this work, the data are first de-multiplexed into separate streams at the transmitter, which are then spread over space and time by modulation onto linear dispersion matrices, which are chosen to maximize the mutual information between the transmitter and receiver.

After the work of Zheng and Tse on the diversity - multiplexing tradeoff, it was naturally of interest to discover the design criteria and practical coding schemes that can achieve the full tradeoff. It soon became clear from the work of Yao and Wornell [61], and Tavildar and Vishwanath [45], that the rank and determinant criteria [44] were a sufficient condition for achieving the full tradeoff. A few of the early schemes which were proposed for the simplest 2×2 MIMO systems, sought to maximize the minimum determinant of the codeword difference matrices, combined with the use of

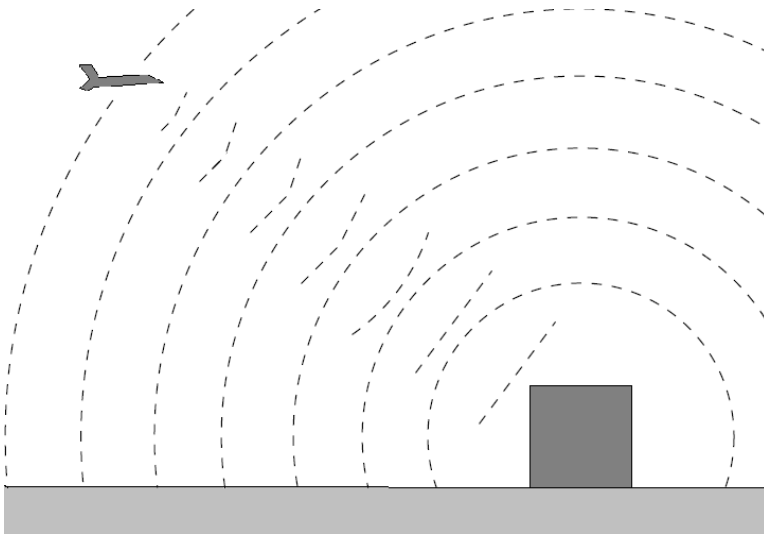


Figure 1.2: The basic principle of radar.

linear dispersion coding [8, 61]. But the signal processing required by some schemes that achieve the optimal tradeoff have a high processing cost, since these schemes require maximum-likelihood decoding, even though the sphere decoding algorithm can often enormously reduce the complexity of ML-decoding [57]. The design of coding schemes that achieve the optimal tradeoff for arbitrary antenna pairs with low processing cost remains an open problem.

1.4 Applications of Antenna Arrays in Radar

Antennas arrays have been used for radar for over three decades. A comprehensive summary of the first two decades can be found in [23]. The benefit from using multiple sensors is greater accuracy for parameter estimation and lower probability of false alarm. Some of the early developments in MIMO research were inspired by the use of antenna arrays for beamforming, the so-called smart antenna arrays [30, 59].

In radar applications, a known waveform is transmitted which is reflected from the target and processed to determine several signal parameters of interest. In military, airport and satellite telemetry applications, the parameters of interest are usually the location and velocity of a target. Radar is also commonly used to determine weather conditions in a wide area. In this case, the signal parameters of interest are the type of precipitation (eg. rain, hail or snow), wind speed/rotation, and other weather conditions. Antenna arrays are also used for microwave imaging in medical applications [26], where differentiation between various tissues is the problem of interest.

The gains from using polarization sensitive elements in radar arrays has been under investigation for at least a decade [58]. A general EM wave has six field components at any point in space, three electric and three magnetic field components. However, the EM plane wave propagating through free space, has only four field components, two electric and two magnetic field components. In our work, we quantify the gain for radar from using a polarization-sensitive array over an unpolarized array by comparing the volume within which a target is located for a given level of confidence [9]. The smaller the volume, the better.

1.5 Dissertation Overview

In this dissertation, we investigate fundamental limits on the performance of large antenna arrays in communications and radar applications. A common thread running through all our results is the use of asymptotic analysis of large antenna arrays to gain insights into finite array behavior. This approach is often useful, because, the asymptotic results are simpler and more transparent than the exact results for finite arrays.

We have already seen how the mutual information in a MIMO communication system can be considered as a random variable dependent on the current channel state information. In order to compute the outage capacity, it is necessary to know the distribution of the mutual information over the ensemble of all channel realizations. A closed-form formula for the distribution was already presented by Telatar [46], but it is relatively complex and does not yield any ready insights into some of observed empirical behavior. In particular, several authors have observed without proof that the distribution appears to tend to a Gaussian distribution as the number of antennas grows [14]. In [17], a proof was given for general MIMO arrays in the limit at high and low SNRs.

In Chap. 2, we give a simple formula for the asymptotic distribution of the mutual information random variable as the MIMO array size tends to infinity. The novelty of this result lies in the fact that the classical central limit theorem (CLT) only yields this behavior in the case when either of the antennas arrays at the transmitter or the receiver tends to infinity, but not both. In the case when both arrays tend to infinity, we actually need recent results from random matrix theory which also yields a Gaussian distribution for the mutual information. We present closed-form formulae for the mean and variance of the capacity, from which parameters the Gaussian distribution of the capacity is completely specified at all SNRs. Although these results are valid asymptotically for large MIMO arrays, we observe that they approximate quite accurately the mutual information distribution within a few standard deviations around the mean in finite arrays with as few as 4 antennas at the transmitter and receiver. This is possible because the variance of the distribution depends only on the ratio of the number of antennas at the two ends of the MIMO link. We discuss how the distribution behaves at high and low SNRs.

In Chap.3, we apply the asymptotic MIMO mutual information results to com-

pute the tradeoffs between diversity and multiplexing at finite SNRs. For this we must first redefine the diversity and multiplexing gains for MIMO systems (defined asymptotically at high SNR by Zheng and Tse [63]) for finite SNRs. The asymptotic mutual information distribution may be used to derive the tradeoffs at high outage capacities, which is the regime of practical interest. This restriction on high outage capacities limits the tradeoff to rates close to the maximum ergodic capacity. We notice that at high SNRs the variance of the distribution of MIMO antenna arrays which have unequal antennas remains constant independent of SNR. Curiously, this is not observed in MIMO arrays which have equal antennas, whose variance grows without bound with increasing SNR. This observation leads to different tradeoff behavior in the case of MIMO arrays with equal and unequal antennas. In particular, we notice that our tradeoffs match the Zheng-Tse tradeoff only in the equal-antenna MIMO array case.

We next attempt to find a general modulation scheme which achieves the optimal Zheng-Tse tradeoff for arbitrary MIMO arrays. This is motivated by the observation that linear dispersion coding by a random unitary matrix yields full rank and full diversity codeword difference matrices with probability one. However, the square codeword blocks hitherto considered have an eigenvalue distribution which peaks at the origin, which follows the asymptotic eigenvalue distribution of large square random matrices with i.i.d. entries. So we consider rectangular codeword blocks, which have an eigenvalue distribution which is asymptotically bounded away from zero for large rectangular random matrices. From our empirical simulation results for the 2×2 MIMO array with 2×3 codeword blocks we show that this scheme may indeed achieve the Zheng-Tse tradeoff.

In Chap. 4, we look at antenna arrays from a radar perspective. Here again we consider asymptotic behavior of large arrays, composed of infinitesimal tripole

antennas packed with increasing density on a finite spherical surface of fixed radius. An infinitesimal tripole antenna or a tri-polarized antenna, is composed of three co-located spatially orthogonal infinitesimal dipole antennas which measure all three components of the electric field at that point in space [6]. We choose a spherical surface because of its symmetry, but the approach we describe is perfectly general and may be applied to arrays of any shape. We are interested in locating the range and direction of a target at an arbitrary location in free space.

The maximum-likelihood estimator is commonly used for parameter estimation, but its performance is hard to analyze. Instead, we compute the Cramer-Rao bound which gives a lower bound on the mean squared error of any unbiased estimator. The goal in this case is to quantify the gains from using an array of vector antennas over a uni-polarized antenna array composed of identically oriented dipoles. The limiting array in either case approximates a general tri-polarized or a uni-polarized current distribution on the surface of the sphere. We use ratios of the volume of confidence ellipsoids obtained from the Cramer-Rao bounds to represent the gains by using arrays of polarized antennas. We show that the gain is the lowest when the target is located in the plane perpendicular to the uni-polarized antennas. When the target is located closer to the equator, the polarized array is shown to provide significant gains over the uni-polarized array.

Chapter 2

The Asymptotic Capacity of Multiple-Antenna Rayleigh Fading Channels

The seminal work of Telatar [46] and Foschini and Gans [10] demonstrated that using multiple antennas at the transmitter and receiver can substantially increase the capacity of fading multipath channels. The input distribution that maximises the mutual information is known to be i.i.d. Gaussian. For a particular channel realisation H , the mutual information in nats per second per Hertz (nps/Hz) is given by

$$C(t, r, \rho) = \ln \left| I + \frac{\rho}{t} H H^\dagger \right| \quad (2.1)$$

that depends upon the channel fading path gains H , the signal-to-noise ratio ρ , and the numbers of transmit and receive antennas, t and r , respectively. $C(t, r, \rho)$ may be viewed as a random variable defined on the ensemble of all possible channel matrices. However, the actual operational limit on reliable communication depends on how H evolves with time: If the path gains are ergodic, $C(t, r, \rho)$ can be averaged over many

channel realizations, and the corresponding operational limit is called the *ergodic capacity*

$$C_e(t, r, \rho) = \mathcal{E} [C(t, r, \rho)] . \quad (2.2)$$

If the path gains are static, however, we observe only one channel realization and there is often an irreducible outage probability associated with every positive rate of transmission. For outage probability $0 < q < 1$, reliable communication is limited by the *outage rate*

$$C_q(t, r, \rho) = \sup \{R \geq 0 : \Pr [C(t, r, \rho) < R] \leq q\} . \quad (2.3)$$

Ergodic capacity and outage rates are usually estimated by Monte Carlo methods, since closed-form formulas are not known, except for a few special cases. Telatar [46] obtained a general formula for ergodic capacity in terms of an integral of a series of Laguerre polynomials. Several authors have derived closed-form asymptotic formulas for ergodic capacity in the limit as $t \rightarrow \infty$ and $r/t \rightarrow c > 0$ [5, 14, 36, 46]. These formulas are often more transparent than finite-array results, and provide more insight into the dependence of ergodic capacity on key system parameters. Our aim in this chapter is to provide a more complete description of the asymptotic behavior of $C(t, r, \rho)$.

We determine the asymptotic probability distribution of $C(t, r, \rho)$ as $t \rightarrow \infty$ and $r/t \rightarrow c > 0$. For all $c > 0$, we show that

$$C(t, r, \rho) - t\mu$$

converges in distribution to a zero-mean Gaussian random variable with variance σ^2 , and give closed-form expressions for μ and σ^2 . A similar result has been recently reported in [17]. Our results enable us to derive the first asymptotic formula for outage rates, and also to find a sharper estimate of the error in previously reported

asymptotic formulas for ergodic capacity. Although these formulas are asymptotic, we show through simulations that they are often quite accurate for finite t and r .

This chapter is organized as follows. In Sec 2.1, we introduce preliminary results from random matrix theory, which are used in Sec 2.2 to determine the asymptotic behavior of $C(t, r, \rho)$. We then compare the asymptotic formulas with Monte Carlo estimates of capacity for finite t and r in Sec 2.3, and summarize our conclusions in Sec 2.4.

2.1 Random Matrix Theory

We begin by reviewing results on the asymptotic spectra of large random matrices. Let $H = \{H_{ij}\}$ be an $r \times t$ random matrix with independent, identically-distributed (i.i.d.) complex entries such that $\mathcal{E}\{H_{ij}\} = 0$ and $\mathcal{E}\{|H_{ij}|^2\} = 1$. Consider the $t \times t$ random matrix

$$B_t = \frac{1}{t} H^\dagger A_r H$$

where A_r is a (possibly random) $r \times r$ nonnegative-definite Hermitian matrix and \dagger denotes conjugate-transpose. We are interested in linear spectral statistics of the form

$$f(B_t) = \frac{1}{t} \sum_{j=1}^t f(\lambda_j) = \int f(\lambda) dF_t(\lambda)$$

where $\{\lambda_j\}$ are the eigenvalues of B_t and

$$F_t(\lambda) = \frac{1}{t} |\{j : \lambda_j \leq \lambda\}|$$

is the *empirical eigenvalue distribution* (EED) of B_t . Similarly, let G_r be the EED of A_r .

Several authors have investigated the asymptotic behavior of $f(B_t)$ in the limit as $t \rightarrow \infty$ and $r/t \rightarrow c > 0$. In particular, Silverstein [42, Thrm 1.1] has shown that,

if A_r and H are independent and G_r converges in distribution, almost surely (a.s.), to a fixed distribution G on $[0, \infty)$, then F_t also converges in distribution a.s. to a fixed distribution F . This distribution is most easily given in terms of its Stieltjes Transform

$$m(z) = \int \frac{1}{\lambda - z} dF(\lambda) \quad (2.4)$$

by the implicit relation

$$z = -\frac{1}{m} + c \int \frac{\tau}{1 + m\tau} dG(\tau), \quad (2.5)$$

where for each z in $\mathbf{C}^+ = \{z \in \mathbf{C} : \text{Im}(z) > 0\}$, $m(z)$ is the unique solution of (2.5) in \mathbf{C}^+ .

These results imply a kind of strong law of large numbers for linear spectral statistics, which asserts that under mild conditions on $f(B_t)$ (e.g. f continuous and bounded, or $f(B_t)$ uniformly integrable)

$$f(B_t) \rightarrow \mu = \int f(\lambda) dF(\lambda), \quad \text{a.s.} \quad (2.6)$$

Recently, Bai and Silverstein [2] have refined these asymptotic estimates to provide a corresponding *central limit theorem* for linear spectral statistics:

Lemma 1 (Bai–Silverstein [2, Thrm 1.1]): Suppose

- (a) $H = \{H_{ij}\}$ are i.i.d. with $\mathcal{E}\{H_{11}\} = \mathcal{E}\{H_{11}^2\} = 0$, $\mathcal{E}\{|H_{11}|^2\} = 1$, $\mathcal{E}\{|H_{11}|^4\} = 2$;
- (b) A_r is a non-random Hermitian nonnegative-definite matrix, with EED G_r that converges in distribution a.s. to a fixed G , and the sequence of spectral norms $\|A_r\|$ is bounded;
- (c) f is continuously differentiable with a bounded first derivative, and analytic on an open interval containing $[(\max\{0, 1 - \sqrt{c}\})^2 \liminf_r \underline{\lambda}_r, (1 + \sqrt{c})^2 \limsup_r \bar{\lambda}_r]$, where $\underline{\lambda}_r$ and $\bar{\lambda}_r$ are the smallest and largest eigenvalues of A_r , respectively.

Let $\mu_t = \int f(\lambda) dF^{c_t, G_r}(\lambda)$, where $c_t = r/t$ and $F^{c, G}$ denotes the distribution with Stieltjes Transform (2.5). Then, as $t \rightarrow \infty$ and $c_t \rightarrow c > 0$,

$$t[f(B_t) - \mu_t] \xrightarrow{d} \mathcal{N}(0, \sigma^2) \quad (2.7)$$

where \xrightarrow{d} denotes convergence in distribution, $\mathcal{N}(0, \sigma^2)$ is a real-valued, zero-mean Gaussian random variable with variance

$$\sigma^2 = -\frac{1}{4\pi^2} \int_{\mathcal{C}_y} \int_{\mathcal{C}_x} \frac{f(x)f(y)}{(m(x) - m(y))^2} m'(x)m'(y) dx dy \quad (2.8)$$

and \mathcal{C}_x and \mathcal{C}_y are any closed positive contours that enclose the support of F .

Remark: [2, Thm 1.1] does not explicitly deal with B_t , but rather with the closely related $r \times r$ matrix $C_r = (1/t)A_r^{1/2}HH^\dagger A_r^{1/2}$, where $A_r^{1/2}$ denotes the Hermitian square-root of A_r . Since the spectra of B_t and C_r differ only in $|t-r|$ zero eigenvalues, we have

$$f(B_t) = (1 - c_t)f(0) + c_t f(C_r) .$$

If $f(B_t) \rightarrow \mu$ almost surely, then $f(C_r) \rightarrow \bar{\mu}$, where $\bar{\mu} = \lim_r \bar{\mu}_r$ and $\mu_t = (1 - c_t)f(0) + c_t \bar{\mu}_r$. [2, Thm 1.1] asserts that $r[f(C_r) - \bar{\mu}_r] \xrightarrow{d} \mathcal{N}(0, \sigma^2)$ as $t \rightarrow \infty$ and $c_t \rightarrow c$. Observing that $t[f(B_t) - \mu_t] = r[f(C_r) - \bar{\mu}_r]$, we conclude that (2.7) also holds.

2.2 Asymptotic Capacity Distribution

We now use the results above to characterize the asymptotic probability distribution of capacity (2.1) in the limit as the number of transmit and receive antennas grows large.

Consider a baseband channel in which t transmit antennas send data to r receive antennas. Let X_{jl} be the complex signal sent from transmit antenna $j = 1, \dots, t$ at

time $l = 1, \dots, n$. Under flat-fading conditions, this signal arrives at receive antenna i multiplied by a fading path gain H_{ij} , and corrupted by additive noise N_{il} . Collecting the signals into a $t \times n$ matrix X , we write the channel as

$$Y = \sqrt{\rho/t}HX + N, \quad (2.9)$$

where Y is an $r \times n$ matrix of received samples, H is the $r \times t$ matrix of fading path gains, and N is an $r \times n$ matrix of noise. We assume the elements of N and H are i.i.d. $\mathcal{CN}(0, 1)$ complex Gaussian random variables and the transmitted signals are normalized to unit power, $(1/tn) \sum_{j=1}^t \sum_{l=1}^n |X_{jl}|^2 = 1$, so that ρ represents the signal-to-noise ratio (SNR) per receive antenna. For simplicity, we first restrict attention to $r \leq t$, so that $c = r/t \leq 1$. This restriction is removed later.

For a given H , the mutual information (2.1) can be written as a linear spectral statistic

$$C(t, r, \rho) = \sum_{i=1}^t \ln(1 + \rho\lambda_i) = t \int_0^\infty \ln(1 + \rho\lambda) dF_t(\lambda),$$

where F_t is the EED of $(1/t)H^\dagger H$. Sec 2.1 characterizes the asymptotic distribution of $C(t, r, \rho)$: In this case, we have $A_r = I_r$ so that $G_r(\lambda) = u(\lambda - 1)$. As $t \rightarrow \infty$ with $r = ct$, the distribution F_t converges almost surely in distribution to a fixed limit F , which has been discussed in previous papers [36, 46, 56]. From (2.5), the Stieltjes transform is

$$m(z) = \sqrt{\left(\frac{1}{2} + \frac{1-c}{2z}\right)^2 - \frac{1}{z} - \frac{1}{2} - \frac{1-c}{2z}}, \quad (2.10)$$

and the limiting distribution has probability density function (pdf)

$$F'(\lambda) = \begin{cases} (1-c)\delta(\lambda) + \frac{1}{2\pi\lambda} \sqrt{(b(c) - \lambda)(\lambda - a(c))}, & a(c) < \lambda < b(c) \\ 0, & \text{otherwise.} \end{cases}$$

where $a(c) = (1 - \sqrt{c})^2$ and $b(c) = (1 + \sqrt{c})^2$.

It is well known that the linear spectral statistic $(1/t)C(t, r, \rho)$ satisfies the conditions required for (2.6), and thus converges almost surely (by Lemma 1) to the fixed limit

$$\begin{aligned}\mu(c, \rho) &= \int_0^\infty \ln(1 + \rho\lambda) dF(\lambda) \\ &= c \ln\{1 + \rho - \rho v(c, \rho)\} + \ln\{1 + \rho c - \rho v(c, \rho)\} - v(c, \rho)\end{aligned}$$

where

$$v(c, \rho) = \frac{1}{2} \left[1 + c + \frac{1}{\rho} - \sqrt{\left(1 + c + \frac{1}{\rho}\right)^2 - 4c} \right]. \quad (2.11)$$

This closed-form formula follows from [56, eqs. 9,38] by setting $\beta = c$ and observing $\mathcal{F}(\rho, c) = 4\rho v(c, \rho)$, or alternatively from [36, eq. 6] by setting $y = c$, $\sigma^2 = 1/\rho$, and observing $v_y = c/w_y = v(c, \rho)$.

It is easy to verify that $C(t, r, \rho)$ also satisfies the hypotheses of Lemma 1. Condition (a) follows from our assumptions on the channel matrix H . Condition (b) is true because $A_r = I_r$ and thus has a fixed EED = $\delta(\lambda - 1)$ and spectral norm = 1 for all r . Condition (c) is satisfied because $f(\lambda) = \log(1 + \rho\lambda)$ which has a unique pole at $\lambda = -1/\rho$ and is hence analytic on the specified interval which lies completely on the positive λ axis.

Thus, as $t \rightarrow \infty$ with $r = ct$, $C(t, r, \rho) - t\mu(c, \rho)$ converges in distribution to a $\mathcal{N}(0, \sigma^2)$ random variable, where from (2.8)

$$\sigma^2 = - \int_{\mathcal{C}_y} \int_{\mathcal{C}_x} \frac{\ln(1 + \rho x) \ln(1 + \rho y)}{4\pi^2(m(x) - m(y))^2} m'(x)m'(y) dx dy \quad (2.12)$$

$m(z)$ is given by (2.10), and \mathcal{C}_x and \mathcal{C}_y are any closed positive contours that contain $[a(c), b(c)]$ but not $-1/\rho$. In Appendix A, we show that this integral can be evaluated as

$$\sigma^2(c, \rho) = - \ln \left[1 - \frac{v^2(c, \rho)}{c} \right]. \quad (2.13)$$

In Appendix B, we show that the variance can equivalently be written in terms of the ergodic capacity as

$$\sigma^2(c, \rho) = \log \left[\frac{\rho^2 \mu''(\rho) - 1}{(\rho \mu'(\rho) - 1)^2} \right] \quad (2.14)$$

We conclude that an asymptotically exact formula for the ergodic capacity is

$$C_e(t, r, \rho) = t\mu(c, \rho) + o(1) . \quad (2.15)$$

where $o(t^k)$ denotes an error term such that $o(t^k)/t^k \rightarrow 0$ as $t \rightarrow \infty$. This asymptotic formula was given previously by Telatar [46] (in integral form) and in [36, 56], where it is proved

$$\lim_{t \rightarrow \infty, r=ct} \frac{C_e(t, r, \rho)}{t\mu(c, \rho)} = 1 ,$$

which is equivalent to an error term of $o(t)$ in (2.15). Using Lemma 1, we have proved the stronger result

$$\lim_{t \rightarrow \infty, r=ct} [C_e(t, r, \rho) - t\mu(c, \rho)] = 0 ,$$

which shows that (2.15) captures the precise asymptotic behavior of the ergodic capacity.

The asymptotic normality of $C(t, r, \rho)$ also leads to a formula for outage rate: As $t \rightarrow \infty$ with $r = ct$, we have for all $0 < q < 1$

$$C_q(t, r, \rho) = t\mu(c, \rho) - x_q \sigma(c, \rho) + o(1) \quad (2.16)$$

where x_q is the unique solution of

$$\operatorname{erfc} \left(x_q / \sqrt{2} \right) = 2q$$

and erfc is the complementary error function. In particular, $x_{0.1} = 1.2816$, $x_{0.05} = 1.6449$, and $x_{0.01} = 2.3263$ give the 10%, 5%, and 1% outage rates, respectively.

Thus far, we have restricted attention to $t \geq r$. However, the results extend easily to $t < r$ using the reciprocity property [46]: Note that $\ln |I_r + (\rho/t)HH^\dagger| =$

$\ln |I_t + (\rho/t)H^\dagger H|$ implies $C(t, r, \rho) = C(r, t, c\rho)$. It follows that (2.15) and (2.16) apply to $t < r$ provided $\mu(c, \rho)$ is replaced by $c\mu(c^{-1}, c\rho)$, and $\sigma(c, \rho)$ is replaced by $\sigma(c^{-1}, c\rho)$. Since $v(c^{-1}, c\rho) = (1/c)v(c, \rho)$, it is easily verified that $c\mu(c^{-1}, c\rho) = \mu(c, \rho)$ and $\sigma(c^{-1}, c\rho) = \sigma(c, \rho)$. Thus both formulas are valid as written for $c > 1$.

The formulas above show that, asymptotically, there is a constant gap between the outage rate and ergodic capacity:

$$\lim_{t \rightarrow \infty, r=ct} [C_e(t, r, \rho) - C_q(t, r, \rho)] = x_q \sigma(c, \rho) .$$

This gap has some unusual properties. For small ρ the gap is proportional to SNR

$$\sigma(c, \rho) \approx \rho\sqrt{c}$$

and grows as r increases or t decreases. However, for large ρ the asymptotic behavior depends on whether there is an equal number of transmit and receive antennas: For $r = t$ and large ρ , the gap behaves as

$$\sigma(1, \rho) \approx \sqrt{(1/2) \ln(\rho/4)}$$

which grows without bound. In sharp contrast, for $c \neq 1$ the gap is independent of SNR for large ρ

$$\sigma(c, \rho) \approx \sqrt{-\ln(1 - \min\{c, c^{-1}\})}$$

and grows without bound as $c \rightarrow 1$. For large ρ , the gap is therefore symmetric in t and r and largest when $t = r$. In a similar way, for fixed ρ the gap behaves as

$$\sigma(c, \rho) \approx \frac{\rho\sqrt{c}}{1 + \rho}$$

for small c and as

$$\sigma(c, \rho) \approx \frac{1}{\sqrt{c}}$$

for large c . Thus, when receive antennas greatly outnumber transmit antennas, the gap is again independent of SNR.

2.3 Numerical Results

Although the results of Sec. 2.2 deal only with the large- t limit, the resulting asymptotic formulas are often surprisingly accurate for finite t , even for relatively small arrays.

In Fig. 2.1, we plot Monte Carlo estimates of the ergodic capacity in bits per second per Hertz (bps/Hz) versus the SNR per bit at each receive antenna

$$E_b/N_0 = \frac{\rho}{C_e(t, r, \rho)}$$

for $t = r = 1, 2, 4, 8$ and 16 . Also plotted for comparison are the values predicted by the asymptotic formula (2.15) for $c = r/t = 1$. Note that the relative error between the predicted and actual values is less than 1% for all $r, t \geq 4$, and the absolute error is less than 0.5 bps/Hz in the range of interest. Similarly, we plot the 10% and 1% outage rates predicted by (2.16) in Figs. 2.2 and 2.3, respectively, along with the corresponding Monte Carlo estimates. Here relative error is less than 5% for all $r, t \geq 4$, and absolute error is less than 3 bps/Hz over the range of interest. For $t = r \leq 2$, the relative error is significantly higher (nearly 30% for $t = r = 1$ in Fig. 2.2) since the distribution of $C(t, r, \rho)$ is far from Gaussian.

Agreement with the asymptotic formulas is even more striking when there are different numbers of transmit and receive antennas. In Figs. 2.4, 2.5 and 2.6, we plot Monte Carlo estimates for $t = 2r = 2, 4, 6, 8$ of the ergodic capacity, 10% and 1% outage rates, respectively, as well as the values predicted by the asymptotic formulas for $c = 1/2$. In Fig. 2.7, 2.8, and 2.9, we show the corresponding plots for $t = 4r = 4, 8, 12, 16$ and $c = 1/4$. In all of these cases, we find remarkably close agreement between the actual capacities and the asymptotic formulas, often to within the thickness of the plot lines. This close agreement is fortuitous for small arrays, where the distribution of capacity is not close to Gaussian.

In Fig. 2.10 we plot the standard deviation of the mutual information as a function of SNR for an increasing sequence of equal antenna MIMO systems. While all the experimental curves match closely with the asymptotic curve at low SNRs, it is seen that as the MIMO array size increases, they agree with the asymptotic curves at higher and higher SNRs. This also explains why the outage capacity approximations are not very accurate at high SNRs in the equal antenna MIMO array cases in Figs. 2.2 and 2.3.

In Fig. 2.11 we plot the standard deviation of the mutual information as a function of SNR for a sequence of MIMO systems with increasing $c = r/t$, starting from $c = 4/24 = 1/6, 1/3, 1/2, 2/3$ to $24/24 = 1$. It is seen that for unequal antenna arrays ($c \neq 1$), the exact curves agree with the asymptotic curves at all SNRs. Correspondingly in Figs. 2.5,2.6,2.8,2.9, it is seen that the outage capacity approximations are tight at all SNRs. We have also plotted (dash-dot line) the limiting standard deviation for unequal MIMO systems at high SNRs, $\sigma(c) = \sqrt{-\ln(1 - \min\{c, c^{-1}\})}$. It can be seen that even the actual variances tend to the same limit.

2.4 Conclusions

We have characterized the asymptotic probability distribution of the capacity of a multiple-antenna Rayleigh fading channel, in the limit as the numbers of transmit and receive antennas become large. The distribution converges to a Gaussian distribution with mean and variance given in closed-form by (2.15) and (2.13), respectively. These results allow us to derive the first asymptotic formula for outage rates, as well as a sharper asymptotic formula for ergodic capacity than has been previously reported in [46] (whose closed form was evaluated in [56], [36]). Although these formulas are asymptotic, simulations suggest they are often remarkably accurate for finite t and

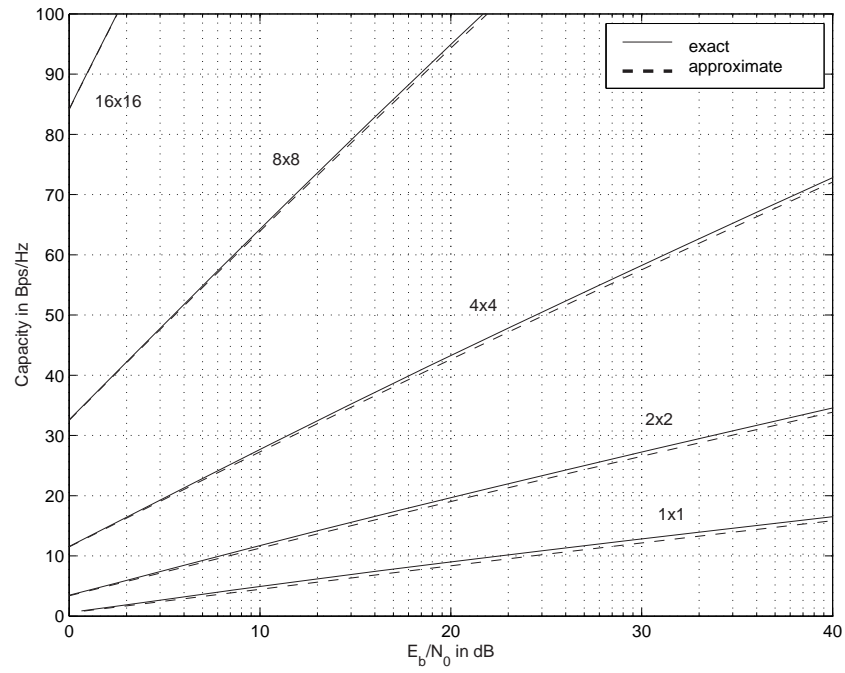


Figure 2.1: Ergodic capacity for $t \times r = 1 \times 1, 2 \times 2, 4 \times 4, 8 \times 8$ and 16×16 .

r . In particular, for all of our simulations with $t, r \geq 4$, the asymptotic formulas are within 5% relative error of the true ergodic capacity and outage rate for $t = r$, and within 0.5% relative error for $t \neq r$.

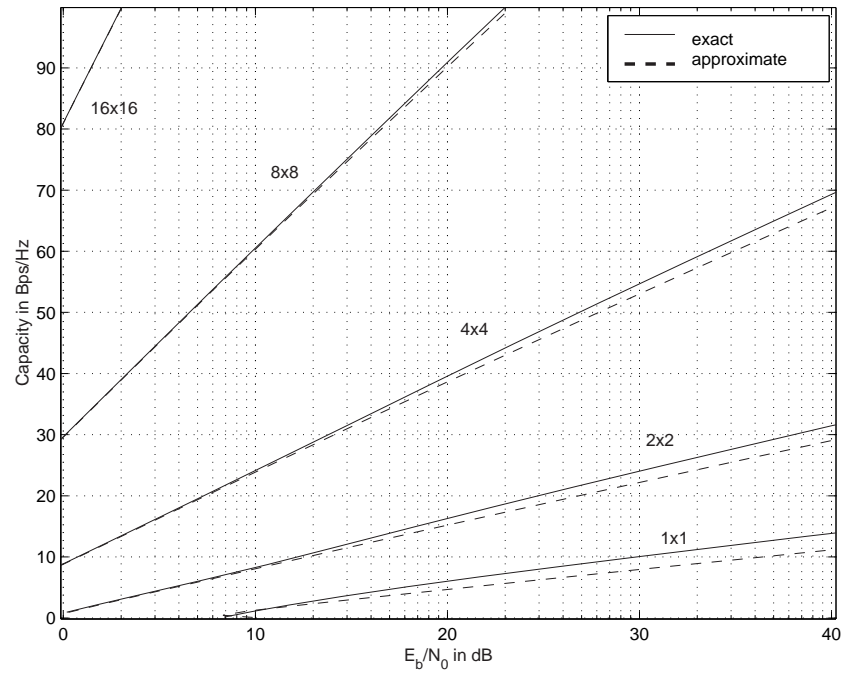


Figure 2.2: 10% outage rate for $t \times r = 1 \times 1$, 2×2 , 4×4 , 8×8 and 16×16 .

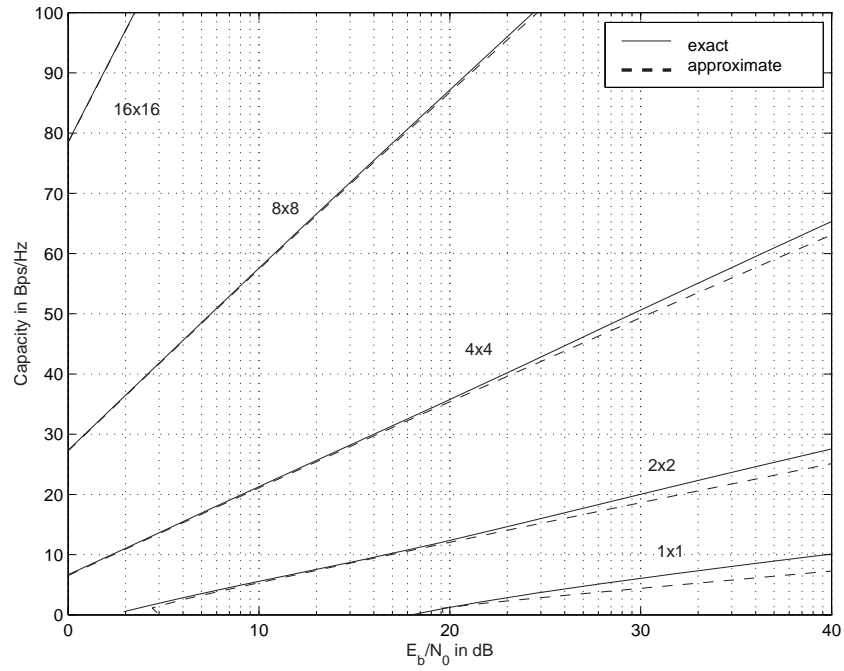


Figure 2.3: 1% outage rate for $t \times r = 1 \times 1$, 2×2 , 4×4 , 8×8 and 16×16 .

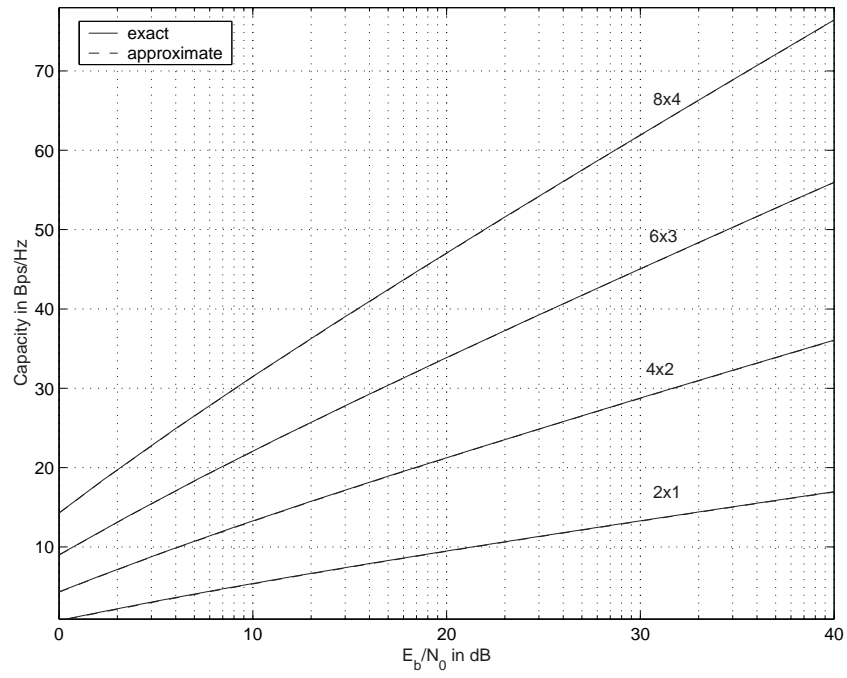


Figure 2.4: Ergodic capacity for $t \times r = 2 \times 1, 4 \times 2, 6 \times 3$ and 8×4 .

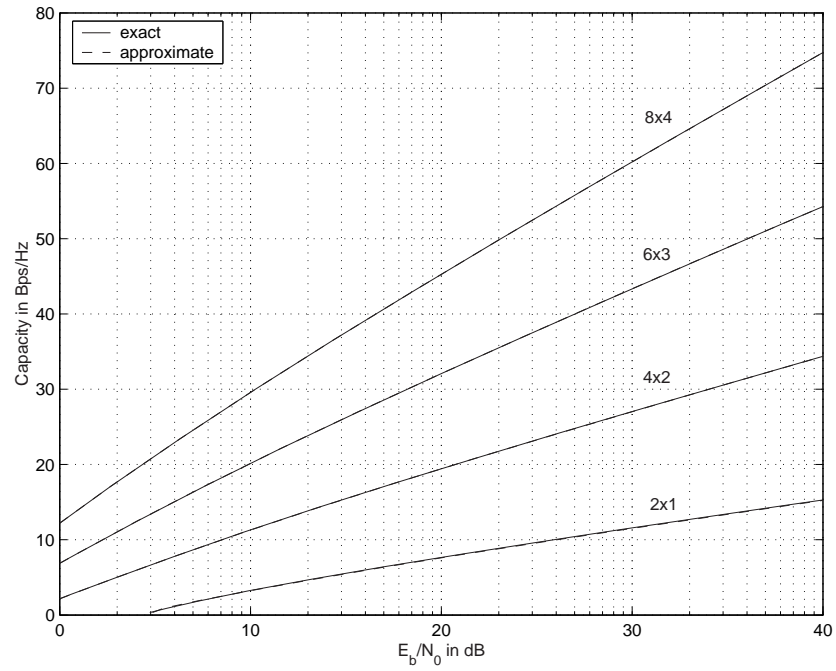


Figure 2.5: 10% outage rate for $t \times r = 2 \times 1, 4 \times 2, 6 \times 3$ and 8×4 .

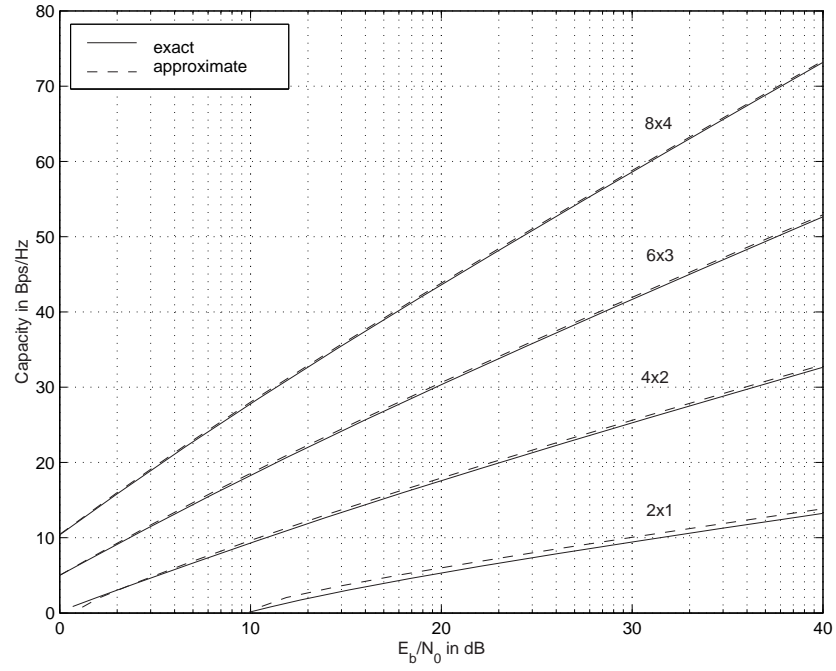


Figure 2.6: 1% outage rate for $t \times r = 2 \times 1, 4 \times 2, 6 \times 3$ and 8×4 .

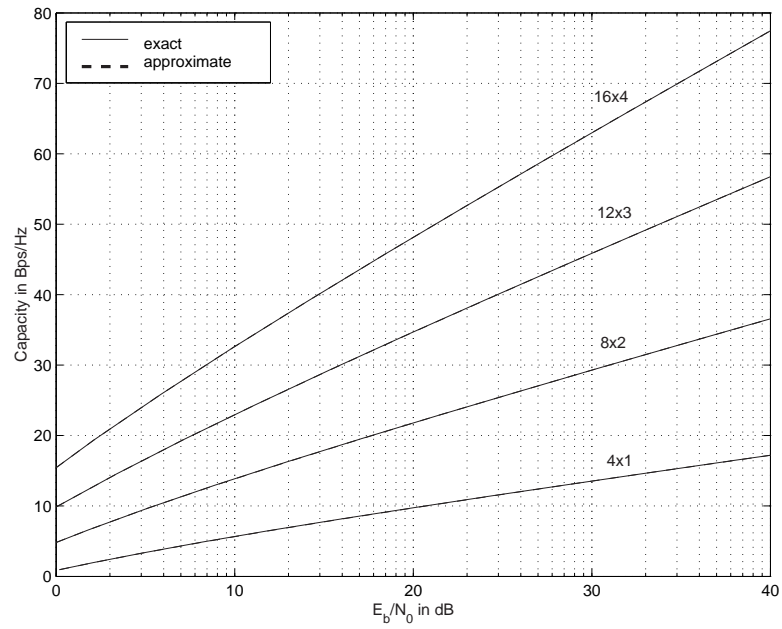


Figure 2.7: Ergodic capacity for $t \times r = 4 \times 1, 8 \times 2, 12 \times 3$ and 16×4 .

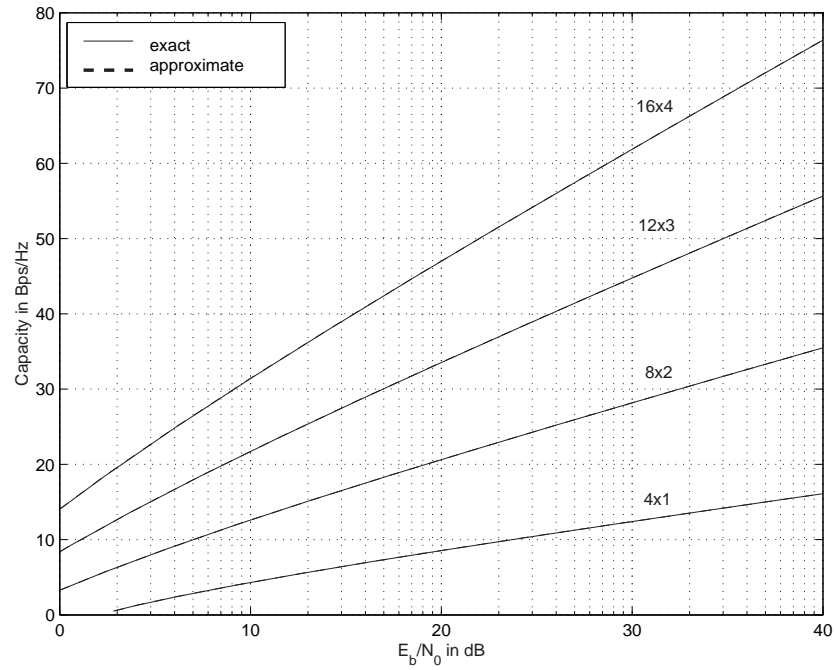


Figure 2.8: 10% outage rate for $t \times r = 4 \times 1$, 8×2 , 12×3 and 16×4 .

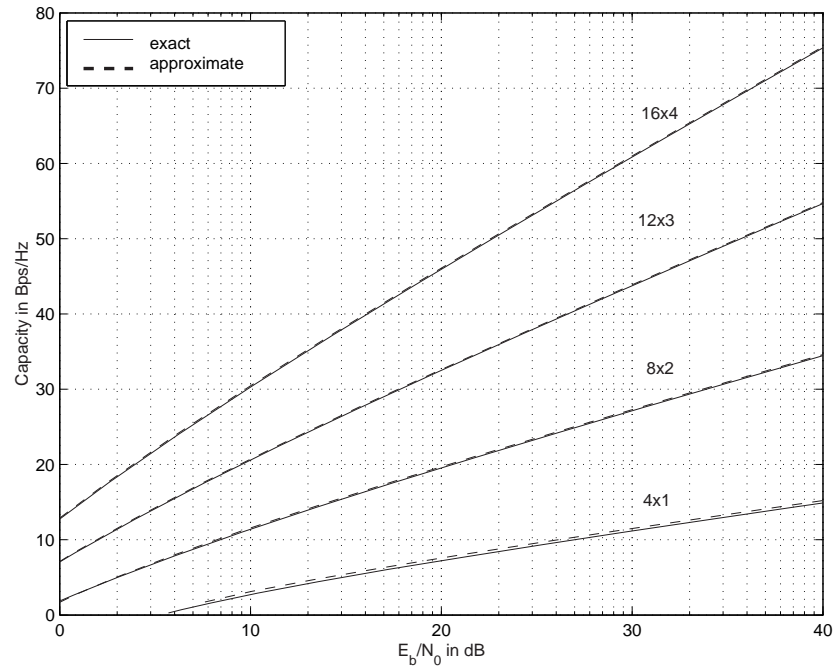


Figure 2.9: 1% outage rate for $t \times r = 4 \times 1$, 8×2 , 12×3 and 16×4 .

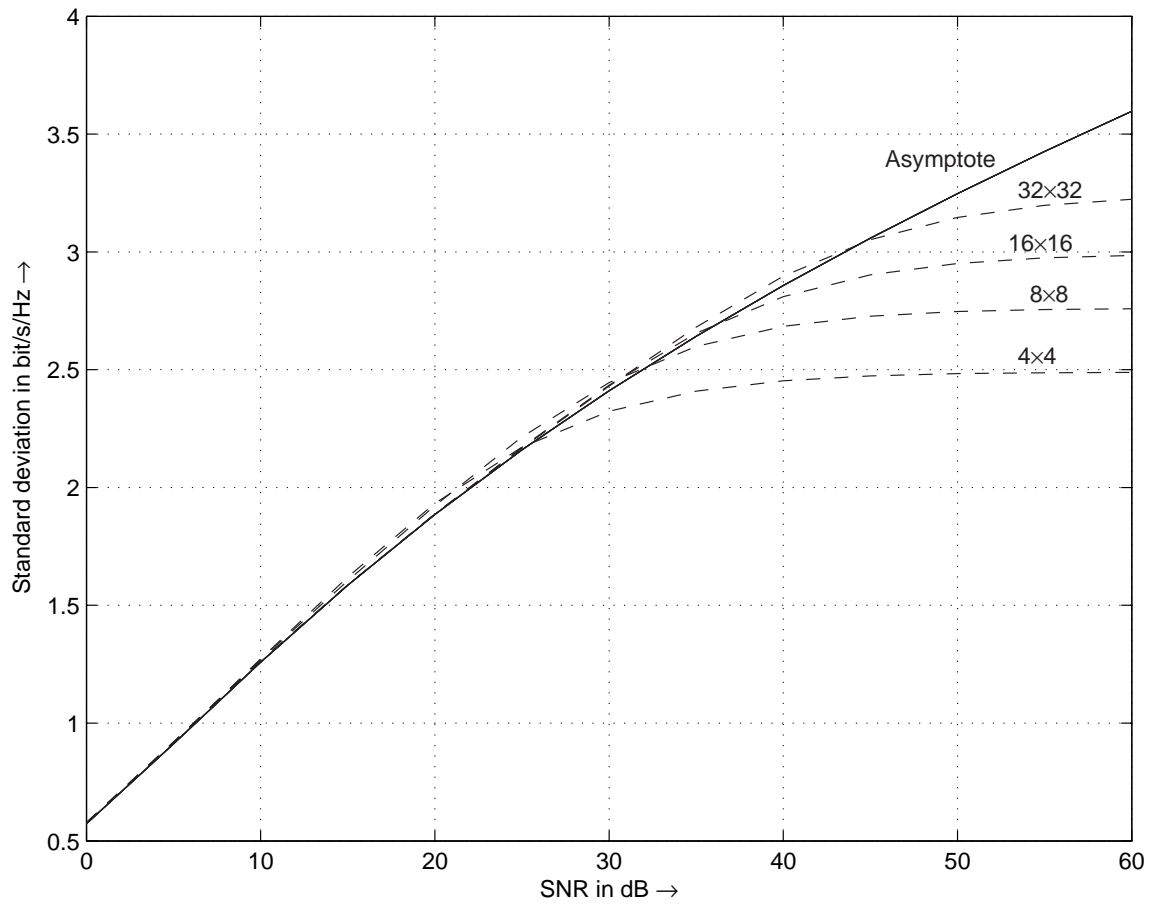


Figure 2.10: Standard deviation of the mutual information for equal antenna MIMO systems.

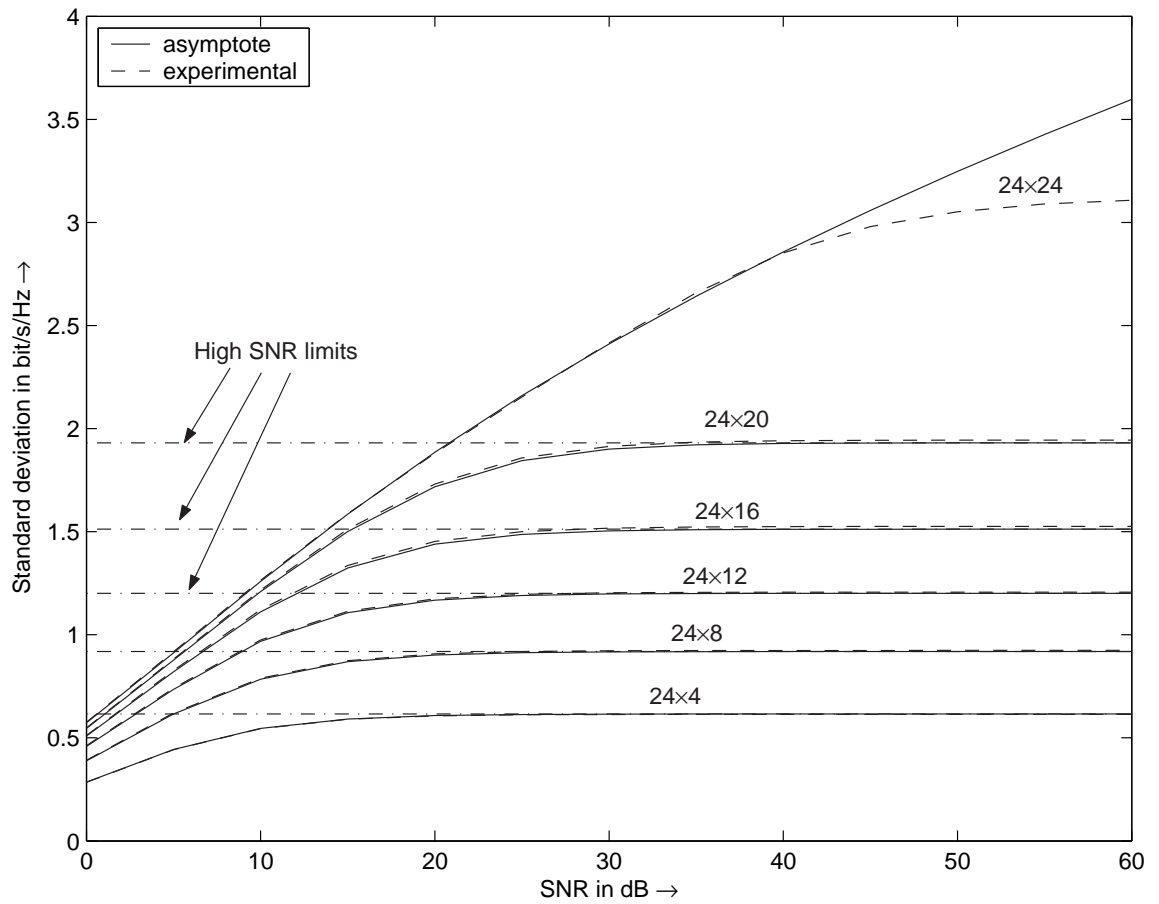


Figure 2.11: Standard deviation of the mutual information for increasing $c = r/t$, starting from $c = 4/24 = 1/6, 1/3, 1/2, 2/3$ to $24/24 = 1$.

Chapter 3

On the Diversity Multiplexing Tradeoff of Large MIMO Arrays

The use of multiple antenna arrays for communication has attracted a lot of attention ever since Telatar [46] and Foschini and Gans [10] demonstrated their substantial benefits in increasing the capacity of fading multipath channels. Intuitively, the gains are due to the fact that by appropriate signal processing, the multiple antennas arrays can be resolved into parallel data pipes. The number of data pipes is usually called the multiplexing gain and well known to be limited by the minimum of the number of antennas on either side of the link. Also, in practice, errors are introduced by the fading multipath channel and additive noise at the receiver. MIMO channels are beneficial in this regard as well, since they provide diversity, which can roughly be described as the number of redundant copies received of the same signal. MIMO systems have a maximum multiplexing gain and also a maximum diversity gain. However, it is not possible to achieve both simultaneously. A number of researchers, most notably Zheng and Tse [63], and others [29], have addressed the tradeoffs between multiplexing and diversity in MIMO communication arrays. In the large MIMO ar-

ray case however, some new wrinkles arise and this chapter tries to address these tradeoffs.

The input distribution that maximizes the mutual information in a MIMO Rayleigh fading channel is known to be i.i.d. Gaussian [46]. For a particular channel realization H , the mutual information in nats per second per Hertz (nps/Hz) is given by $C(t, r, \rho) = \ln |I + \frac{\rho}{t} H H^\dagger|$ that depends upon the channel fading path gains H , the signal-to-noise ratio ρ , and the numbers of transmit and receive antennas, t and r , respectively. $C(t, r, \rho)$ may be viewed as a random variable defined on the ensemble of all possible channel matrices. However, the actual operational limit on reliable communication depends on how H evolves with time: If the path gains are ergodic, $C(t, r, \rho)$ can be averaged over many channel realizations, and the corresponding operational limit is called the *ergodic capacity* $C_e(t, r, \rho) = \mathcal{E} [C(t, r, \rho)]$. If the path gains are static, however, we observe only one channel realization and there is often an irreducible outage probability associated with every positive rate of transmission. For outage probability $0 < q < 1$, reliable communication is limited by the *outage rate* $C_q(t, r, \rho) = \sup \{R \geq 0 : \Pr [C(t, r, \rho) < R] \leq q\}$.

In Chap. 2, we determined the asymptotic probability distribution of $C(t, r, \rho)$ as $t \rightarrow \infty$ and $r/t \rightarrow c > 0$. We showed that, for all $c > 0$, $C(t, r, \rho) - t\mu$ converges in distribution to a zero-mean Gaussian random variable with variance σ^2 , and gave closed-form expressions for μ and σ^2 . A similar result was reported in [17]. Although these formulas are asymptotic, we showed through simulations that they are often quite accurate for finite t and r .

In the terminology of the papers [29, 63] which address the diversity/multiplexing tradeoffs, the ergodic capacity is treated as a benchmark for the multiplexing gain, and the outage probability gives us the diversity gain. Our asymptotic results enable us to immediately analyze these tradeoffs in the context of large MIMO arrays.

This chapter is organized as follows. In Sec. 3.1, we discuss the diversity multiplexing tradeoffs in the context of large MIMO array systems. In Sec. 3.2 we describe a scheme which may achieve the full Zheng-Tze diversity multiplexing tradeoff for finite antenna arrays. We summarize our results in Sec. 3.3.

3.1 Large Array Tradeoffs

Consider a baseband channel in which t transmit antennas send data to r receive antennas. Let X_{jl} be the complex signal sent from transmit antenna $j = 1, \dots, t$ at time $l = 1, \dots, n$. Under flat-fading conditions, this signal arrives at receive antenna i multiplied by a fading path gain H_{ij} , and corrupted by additive noise N_{il} . Collecting the signals into a $t \times n$ matrix X , we write the channel as

$$Y = \sqrt{SNR/t}HX + N, \quad (3.1)$$

where Y is an $r \times n$ matrix of received samples, H is the $r \times t$ matrix of fading path gains, and N is an $r \times n$ matrix of noise. We assume the elements of N and H are i.i.d. $\mathcal{CN}(0, 1)$ complex Gaussian random variables and the transmitted signals are normalized to unit power, $(1/tn) \sum_{j=1}^t \sum_{l=1}^n |X_{jl}|^2 = 1$, so that SNR represents the signal-to-noise ratio per receive antenna. In Chap. 2, we represented SNR by the symbol ρ . We shall use the two variable names interchangeably in this chapter, but it is to be understood that they are referring to the same quantity. To simplify the exposition, we restrict our attention to $r \leq t$, so that $c = r/t \leq 1$. The results for $c > 1$ can be derived similarly through reciprocity, which we discussed in Chap. 2.

In a non-fading AWGN communication channel using BPSK, the error probability for an uncoded data stream is given by, $P_e = Q(\sqrt{E_b/2N_0})$ where the E_b is the energy per bit and N_0 is the level of the noise power spectral density. At high SNRs, the $Q(\cdot)$ function can be approximated to give $P_e \doteq \exp(-E_b/2N_0)$ (the \doteq notation is explained

below). Thus the error probability in an AWGN channel decreases exponentially with SNR .

In a AWGN Rayleigh fading channel using BPSK, the error probability at a given noise SNR has to be averaged over the fading channel gains and is well known [33] to be of the order of $P_e \approx SNR^{-1}$.

For a single transmit and L receive antennas with L independently fading Rayleigh paths, it can be similarly shown [33] to have an error probability of the order of $P_e \approx SNR^{-L}$. Hence, it is called a L -diversity system to indicate the exponent of the SNR in the error probability bound.

In the MIMO channel with t transmit and r receive antennas with data rate $R(SNR)$, Zheng and Tse [63] defined the *spatial multiplexing gain* m as,

$$\lim_{SNR \rightarrow \infty} \frac{R(SNR)}{\log(SNR)} = m \quad (3.2)$$

and *diversity gain* d in terms of error probability as

$$\lim_{SNR \rightarrow \infty} \frac{\log P_e(SNR)}{\log(SNR)} = -d \quad (3.3)$$

Their main result is summarized in the following theorem.

Theorem: The optimal tradeoff curve is given by the piecewise-linear function connecting the points $(k, d^*(k))$, $k = 0, 1, \dots, \min\{r, t\}$ where

$$d^*(k) = (t - k)(r - k).$$

In particular, the maximum diversity $d_{max}^* = rt$ and maximum multiplexing gain $m_{max}^* = \min(r, t)$. This is shown in Fig. 3.1.

The key to this result is the bound for outage probability defined as

$$P_{out}(R) = P [\log \det (I + SNR/tHH^\dagger) < R]$$

which at high SNR is shown to be $P_{out}(k \log(SNR)) \doteq SNR^{-d^*(k)}$, where the \doteq means of the order of as defined by (3.3).

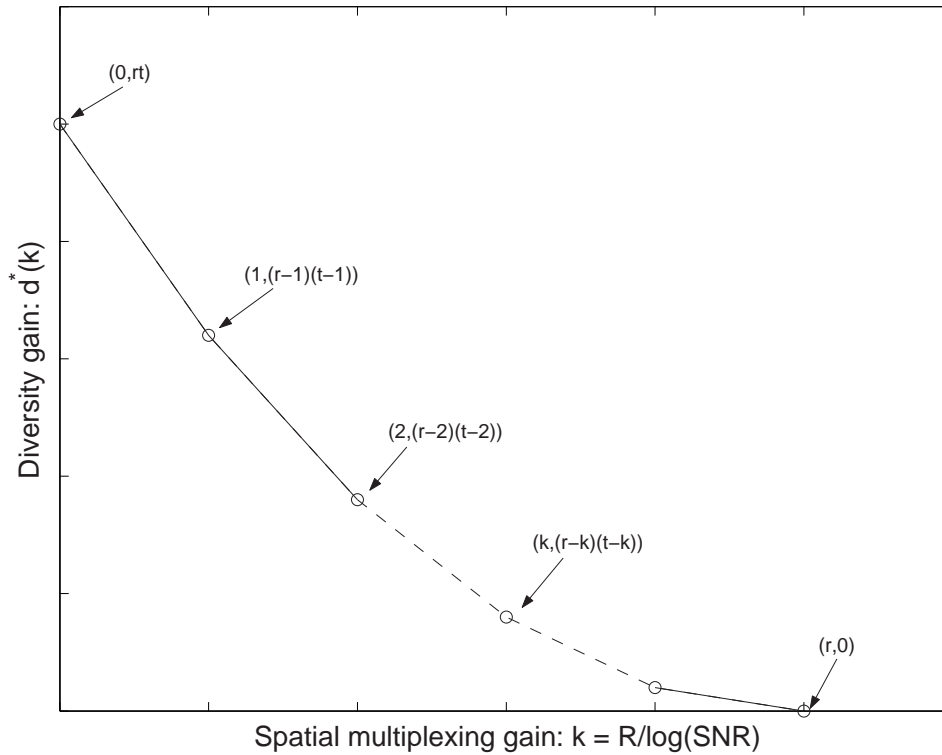


Figure 3.1: The Zheng-Tse diversity multiplexing tradeoff curve.

Since we are interested in tradeoffs at finite SNRs, we need to redefine the multiplexing and diversity gains [38]. We define multiplexing gain as the rate gain over the normalized ergodic capacity μ (here and in the following discussion we have scaled the μ in Chap. 2 by a factor of c^{-1}) at the same SNR,

$$k = \frac{R(\text{SNR})}{\mu(\text{SNR})} \quad (3.4)$$

and the diversity exponent is defined as the negative of the slope of the log-log plot of the outage probability Vs SNR.

$$d = -\frac{\text{SNR}}{P_{out}(\text{SNR})} \frac{\partial P_{out}(\text{SNR})}{\partial \text{SNR}} \quad (3.5)$$

Now we are in a position to apply our results to examine the diversity/multiplexing

tradeoffs of large MIMO arrays. Since we know the asymptotic pdf of the instantaneous data rates is normal $\sim \mathcal{N}(r\mu, \sigma^2)$, the outage probability is simply given by summing the tail of the Gaussian distribution,

$$P_e(k\mu) = Q((r-k)\mu/\sigma). \quad (3.6)$$

From the finite SNR diversity definition (3.5) above, the finite SNR diversity multiplexing tradeoff curve is given by the formula

$$d(k) = \rho(r-k) \frac{\exp\left(-\frac{(r-k)^2\mu^2}{2\sigma^2}\right)}{Q\left(\frac{(r-k)\mu}{\sigma}\right)} \frac{d}{d\rho} \left(\frac{\mu}{\sigma}\right) \quad (3.7)$$

The Gaussian approximation does not yield the complete tradeoff for all rates. The outage probability cannot be computed by this method when $k \ll r$ (for large r). However, we do get the tradeoffs at all SNRs for rates close to $r\mu$. Equivalently, this gives us the tradeoffs in the region of high outage probability, which is typical in practical systems (see Figs. 3.5, 3.6 below). As we noted in Chap. 2, the asymptotics predict the outage capacity for finite antenna arrays with less than 10 antennas on either side of the link quite accurately for outage probabilities up to 10^{-2} . For larger arrays, the asymptotics predict the outage capacities for much smaller outage probabilities.

Next, we compare the tradeoffs obtained by using the large array asymptotics at high SNRs in order to compare them with the Zheng-Tse tradeoff. At high SNRs, the ergodic capacity is given by $r\mu = r \log(SNR)$. However, as observed in Chap. 2, the standard deviation behaves differently at high SNRs depending on two cases. For equal antennas on either side of the link, $r = t$,

$$\sigma \approx \sqrt{1/2 \log(SNR/4)}$$

In sharp contrast, for unequal antennas, we have

$$\sigma \approx \sqrt{-\log(1 - \min\{c, c^{-1}\})}$$

In the limit of large or small c , $\sigma \approx \sqrt{c}$.

Therefore, the high SNR outage probability with equal antennas behaves as

$$P_e(k \log(SNR)) \doteq \exp\left(- (r - k)^2 \frac{\log(SNR)^2}{1/2 \log(SNR/4)}\right)$$

which corresponds to the Zheng-Tse diversity multiplexing tradeoff curve for equal antennas, $d^*(k) = (r - k)^2$.

In the unequal antenna case, the outage probability is given by

$$P_e(k \log(SNR)) \doteq \exp\left(- (r - k)^2 \frac{\log(SNR)^2}{-\log(1 - \min\{c, c^{-1}\})}\right).$$

which is of the order $SNR^{-\log(SNR)}$ and hence does not have a diversity interpretation!

How do we explain the difference in the outage behavior?

First consider the single antenna fading channel case, (we follow the exposition in Zheng-Tse) $y = \sqrt{SNR}hx + n$ where h is Rayleigh distributed and n is AWGN. The outage probability for a target data rate of $R = r \log(SNR)$ ($0 < r < 1$) is

$$\begin{aligned} P_{out}(r \log(SNR)) &= P(\log(1 + SNR||h||^2) < r \log(SNR)) \\ &= P(1 + SNR||h||^2 < SNR^r) \\ &\approx P(||h||^2 < SNR^{-(1-r)}) \end{aligned}$$

Now, since $||h||^2$ is exponentially distributed with density $p_{||h||^2}(x) = e^{-x}$, $P_{out}(r \log(SNR)) \approx P(||h||^2 < SNR^{-(1-r)}) = 1 - \exp(-SNR^{-(1-r)}) \doteq SNR^{-(1-r)}$. Similarly, for the L diversity Rayleigh fading channel, we can show that, $P_{out}(r \log(SNR)) \doteq SNR^{-L(1-r)}$ which gives us the tradeoff between rate and diversity.

We have already seen that the asymptotic diversity-multiplexing tradeoff agrees with the finite antenna results for the equal antennas case. This can be interpreted to

mean that asymptotically, the maximum likelihood estimates of the data streams are distributed Rayleigh-like, so the error probability is proportional to SNR^L , according to the available diversity L .

Let us take another look at the outage probability,

$$\begin{aligned}
P_{out}(R) &= P [\log \det (I + (SNR)/tHH^\dagger) < R = k \log(SNR)] \\
&= P \left[\prod_i (1 + SNR\lambda_i) < SNR^k \right] \\
&= P \left[\prod_i SNR^{(1-\alpha_i)^+} < SNR^k \right] \\
&= P \left[\sum_i (1 - \alpha_i)^+ < k \right]
\end{aligned}$$

where we have made the substitution $\lambda_i = SNR^{-\alpha_i}$ and hence $(1 + SNR\lambda_i) \doteq SNR^{(1-\alpha_i)^+}$.

It is well known [42] that the unordered eigenvalues of $1/tHH^\dagger$ have the limiting distribution

$$F'(\lambda) = \begin{cases} \frac{1}{2\pi c\lambda} \sqrt{(b(c) - \lambda)(\lambda - a(c))}, & a(c) < \lambda < b(c) \\ 0, & \text{otherwise.} \end{cases}$$

where $a(c) = (1 - \sqrt{c})^2$ and $b(c) = (1 + \sqrt{c})^2$. This is shown in Fig[3.2].

Now for equal antenna systems the asymptotic E.E.D.

$$F(\lambda) = \frac{1}{2\pi\lambda} \sqrt{(4 - \lambda)(\lambda)}, 0 < \lambda < 4$$

which implies that the eigenvalues λ_i can lie arbitrarily close to zero. Hence, the Zheng-Tse analysis applies in this case and we get the same tradeoffs.

A result of Silverstein [42] states that for large matrices, the limiting *E.E.D.*, $F'(\lambda)$ has no support outside the interval $\{a(c), b(c)\}$ where $a(c) = (1 - \sqrt{c})^2$ and $b(c) = (1 + \sqrt{c})^2$. This means that for unequal antenna systems, the minimum eigenvalue

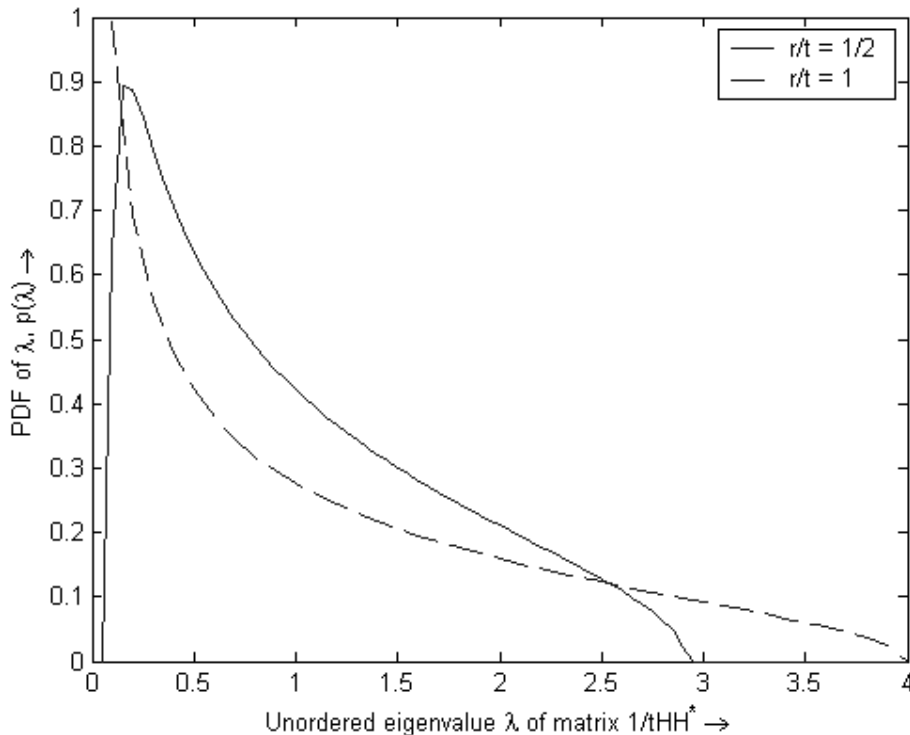


Figure 3.2: Asymptotic empirical eigenvalue distribution(EED) of a $r \times t$ matrix $\frac{1}{t}HH^\dagger$ for two cases, $r = t$ and $2r = t$, as $r, t \rightarrow \infty$.

$\lambda_{min} \geq a(c) = (1 - \sqrt{c})^2$ and hence is strictly bounded away from zero. Therefore, for large $SNRs$, the α_i are distributed arbitrarily close to zero, which implies that $P[\sum_i (1 - \alpha_i)^+ < k] = P[r - \sum_i \alpha_i < k] = P[\sum_i \alpha_i > r - k] = 0$. Therefore, from a strictly diversity viewpoint, we have gotten a result that we already expected: from the Silverstein-Bai limiting distribution, we saw that the outage probability for unequal arrays was given by

$$P_{out}(k \log(SNR)) \doteq \exp\left(- (r - k)^2 \frac{\log(SNR)^2}{-\log(1 - \min\{c, c^{-1}\})}\right),$$

which gives us infinite diversity as $SNR \rightarrow \infty$ which also implies that the limiting outage probability is zero.

We can explain the disparity in the results from the two different approaches as follows: while the Zheng-Tse analysis is concerned only with the ultimate diversity with unlimited SNR, our analysis gives the diversity at finite SNRs and also tells us how it grows with SNR. This could be of help for system design at finite SNRs.

We have plotted the large array diversity multiplexing tradeoff curves for fixed SNRs using formula (3.7), starting from 0dB to 40dB, in steps of 5dB, for equal antenna array MIMO systems $r/t = c = 1$ in Fig. 3.3. We have also plotted the corresponding 4×4 Zheng-Tse tradeoff curve(circled) for comparison. It can be observed that the finite SNR tradeoff curve tends to the Zheng-Tse curve at high SNRs.

In Fig. 3.4, we have plotted the diversity multiplexing tradeoff curves for finite SNRs using formula (3.7) starting from -5 dB to 25dB, in steps of 5dB, for unequal antenna arrays $r/t = c = 1/2$. In this case, we cannot really compare the Zheng-Tse tradeoff curves with the asymptotic curves, because the Zheng-Tse tradeoff curves change with increasing r and t , even if we keep their ratio $r/t = c$ constant. To show this, we have plotted the the Zheng-Tse tradeoff curves(circled) for a 4×2 and a 8×4 system. The asymptotic tradeoff curve tends to a vertical line(infinite diversity) at r in the limit at high SNR, because the diversity increases without limit with increasing SNR for rates less than the ergodic capacity.

In order to achieve the Zheng-Tse tradeoff, we need to design coding schemes over an increasing sequence of rates. The information theoretic outage probability curves give us an upper bound for the performance of any coding scheme at a given rate. To illustrate the region of validity of our finite SNR tradeoff curves in the finite array regime, we have plotted the actual outage probability curves for a 4×4 MIMO system obtained experimentally for an increasing sequence of rates alongside the curves obtained from the asymptotic formula (3.6) in Fig. 3.5. In Fig. 3.6, we

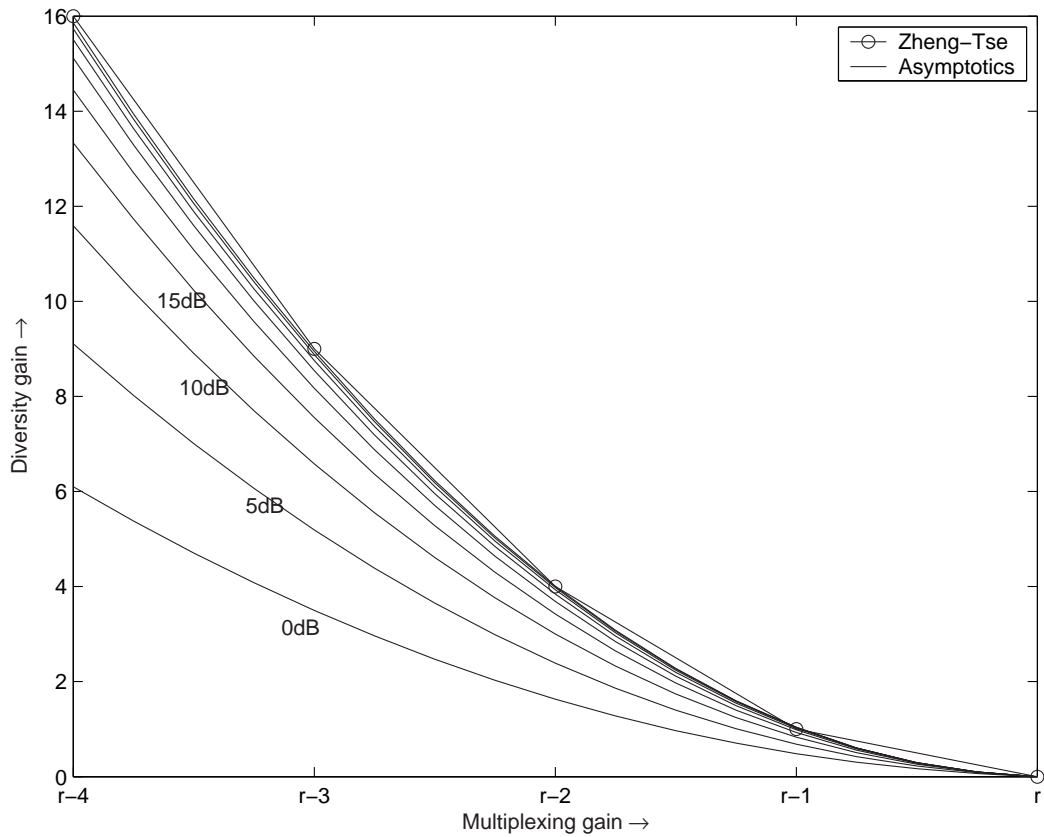


Figure 3.3: Large array asymptotic diversity multiplexing tradeoff curves for fixed SNRs starting from 0dB to 40dB, in steps of 5dB, for equal antenna MIMO arrays compared with the 4×4 MIMO system Zheng-Tse tradeoff.

have plotted experimentally obtained curves for the same increasing sequence of rates for a 8×4 MIMO system alongside the curves obtained from the asymptotic formula (3.6). In both the plots, it can be seen that the predictions match the experimental curves very closely in the low SNR and high outage probability region upto 10^{-2} in all cases (and even for outage probabilities as low as 10^{-4} for some rates).

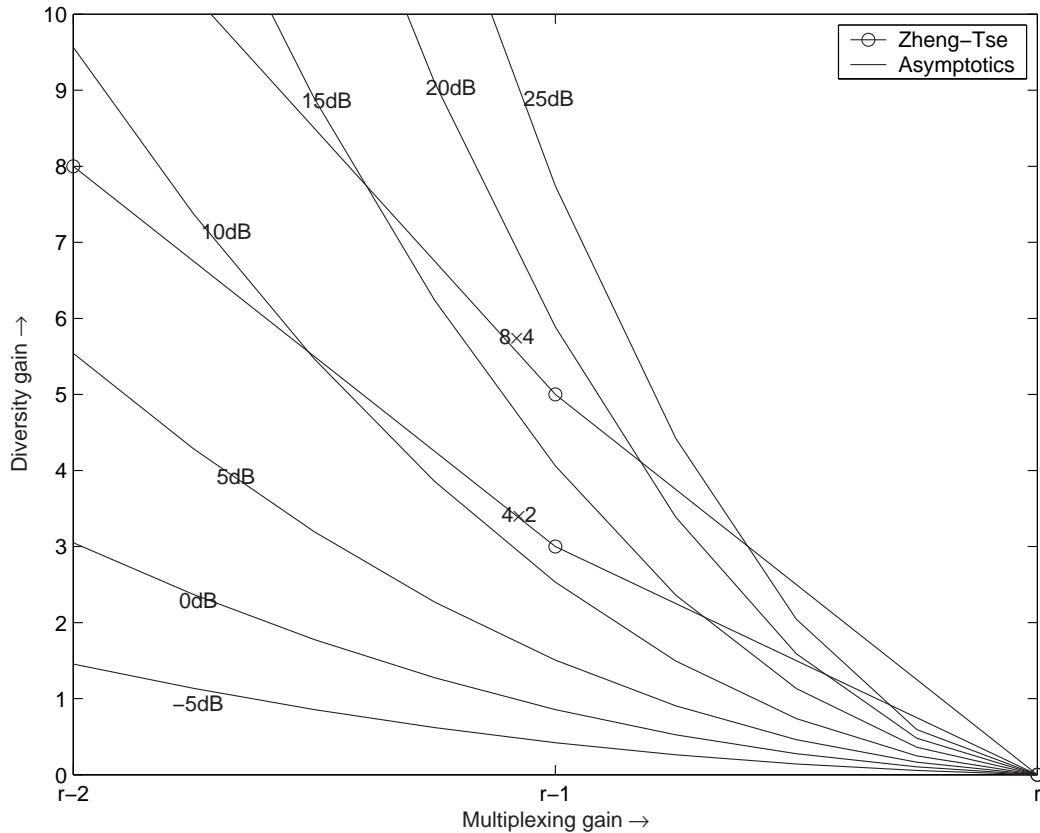


Figure 3.4: Large array asymptotic diversity multiplexing tradeoff curves for fixed SNRs starting from -5dB to 25dB , in steps of 5dB , for unequal antenna MIMO arrays $r/t = c = 1/2$.

3.2 Achieving the Diversity-Multiplexing Tradeoff

In this section we shall discuss how the large random matrix results suggest a coding scheme which may achieve the Zheng-Tse diversity/multiplexing-tradeoff for small arrays. We shall need the following notation, following [54]: *vec*: for a $m \times n$ matrix A , $\text{vec}(A)$ is a vector obtained by stacking successive columns of A on top on one another resulting in a $mn \times 1$ vector. *mat*: for a $mn \times 1$ vector v , $\text{mat}(v, m, n)$ is a matrix obtained by the reverse operation of $\text{vec}()$. (This is identical to the MATLAB function $\text{reshape}(V, m, n)$.)

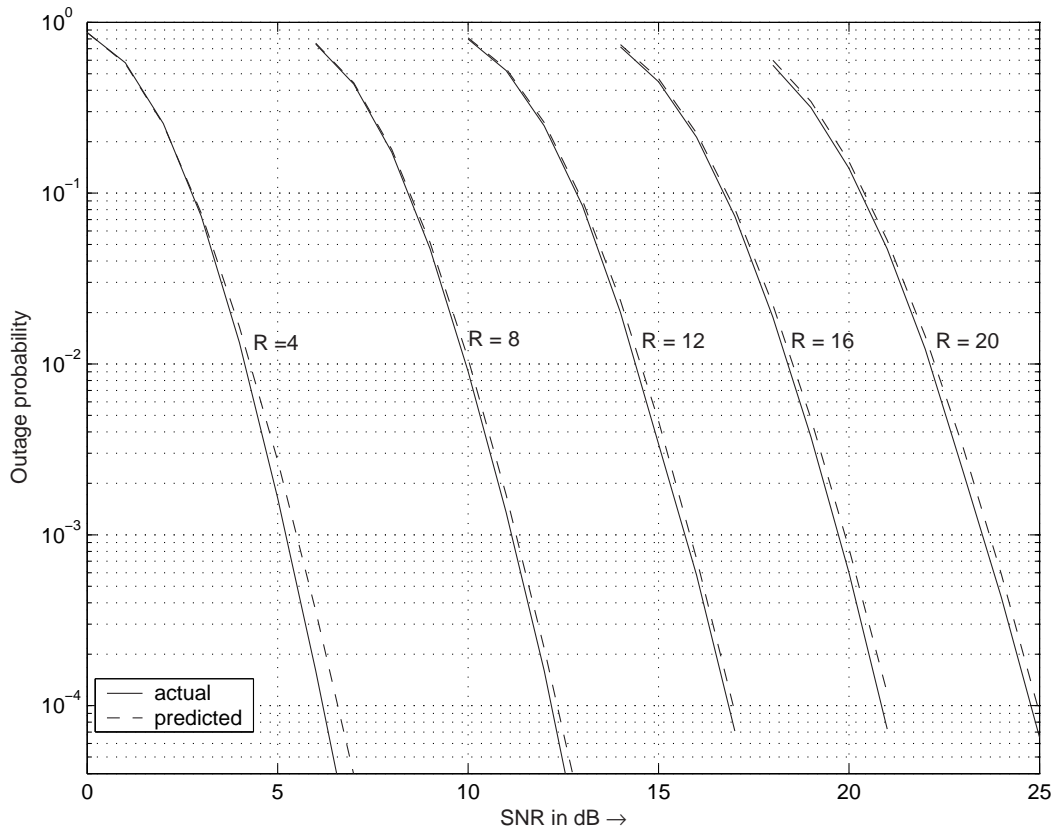


Figure 3.5: Actual outage probability curves for a 4×4 MIMO system obtained experimentally versus the curves predicted by the asymptotic formula (3.6) for an increasing sequence of rates $R = 4, 8, \dots, 20$.

Notice that, while the definition of $vec()$ is unambiguous with respect to $\{m, n\}$, the dimensions need to be specified explicitly in the definition of $mat()$.

Our scheme is a particular case of the linear dispersion codes of [16]. First, observe that a general linear dispersion process can be represented by a $mt \times nt$ matrix A , (with possibly complex entries) which modulates a $t \times n$ block of data X to give a $t \times m$ block of transmitted symbols $X' = mat(A \times vec(X), t, m)$. We shall restrict our attention to square $mt \times mt$ dispersion matrices A .

The Zheng-Tse analysis showed that using Gaussian codebooks, which have the

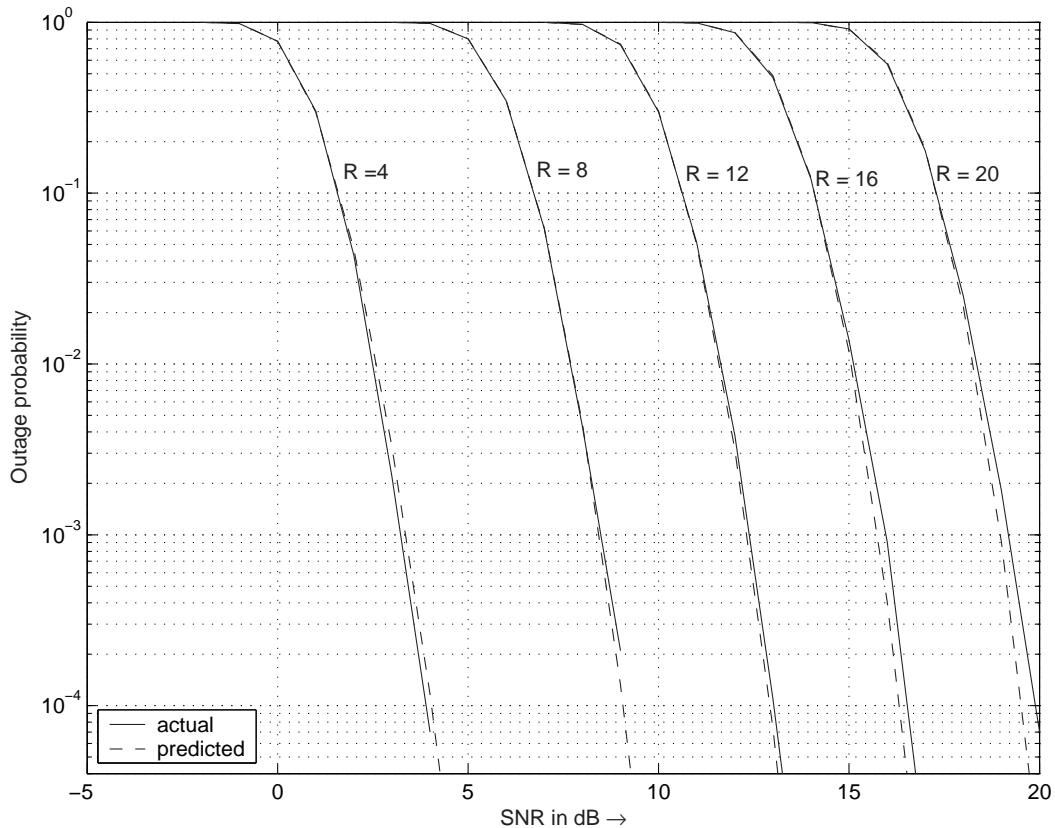


Figure 3.6: Actual outage probability curves for a 8×4 MIMO system obtained experimentally versus the curves predicted by the asymptotic formula (3.6) for an increasing sequence of rates $R = 4, 8, \dots, 20$.

mutual information maximizing distribution ensures that we meet the diversity-multiplexing tradeoff. With Gaussian codebooks, a non-unitary spreading matrix A always leads to penalty in mutual information, because it alters the capacity-achieving input distribution. A unitary dispersion matrix does not change the source distribution or the source eigenvalues. By restricting A to be unitary, the source distribution is unchanged, i.e. it transforms a Gaussian codebook into a Gaussian codebook. So it is clear that dispersion by a unitary matrix achieves the diversity multiplexing tradeoff.

But what have we gained? The difference is that now each source symbol is spread in space over all transmit antennas. Also, unitary modulation enables us to index a matrix Gaussian codebook through a linear Gaussian codebook.

In practice, we can replace the Gaussian codebooks with symbols from an increasing sequence (typically, QAM) of discrete constellations, depending on the rate at which we wish to transmit. It is not obvious that unitary linear dispersion with finite constellations will achieve the tradeoff.

To motivate our case, we shall again invoke the result of Silverstein [42] that we stated earlier. This means that for large arrays, the smallest eigenvalue of the codeword difference matrix is lower bounded by $(1 - \sqrt{c})^2$.

The key is to ensure that the minimum determinant of all codeword difference matrices is bounded away from zero. It can be immediately verified that unitary linear dispersion satisfies all the conditions required for Silverstein's theorem to hold except the entries are not identically distributed. But this too can be ensured by successively using cyclically row-shifted versions of the unitary matrix (known to the receiver). Even though the random matrix results do not directly apply to small MIMO arrays, it is observed that they do reflect in the distribution of the determinant close to the origin (discussed further below).

As an example, consider the smallest possible MIMO system with two-transmit and two-receive antennas. It is known that a minimum block size of $l = m + n - 1$ is sufficient to achieve the full diversity-multiplexing tradeoff. In the 2×2 case, a block size of $3 = l \geq m + n - 1 = 2 + 2 - 1 = 3$ will suffice. Therefore, we pick a 6×6 unitary matrix $U = [u_{ij}]$ at random, to encode blocks of data of size 2×3 . (After a matrix was chosen, it was kept fixed through all of our simulations.) For illustration, the effective system equation for the first three channel use instances can be written

as,

$$\begin{bmatrix} y_{11} \\ y_{21} \\ y_{12} \\ y_{22} \\ y_{13} \\ y_{23} \end{bmatrix} = \begin{bmatrix} h_{11} & h_{12} & 0 & 0 & 0 & 0 \\ h_{21} & h_{22} & 0 & 0 & 0 & 0 \\ 0 & 0 & h_{11} & h_{12} & 0 & 0 \\ 0 & 0 & h_{21} & h_{22} & 0 & 0 \\ 0 & 0 & 0 & 0 & h_{11} & h_{12} \\ 0 & 0 & 0 & 0 & h_{21} & h_{22} \end{bmatrix} \begin{bmatrix} u_{11} & \dots & u_{16} \\ \vdots & \ddots & \vdots \\ u_{61} & \dots & u_{66} \end{bmatrix} \begin{bmatrix} x_{11} \\ x_{21} \\ x_{12} \\ x_{22} \\ x_{13} \\ x_{23} \end{bmatrix} + \begin{bmatrix} z_{11} \\ z_{21} \\ z_{12} \\ z_{22} \\ z_{13} \\ z_{23} \end{bmatrix}$$

where y_{in} represents the output samples at the receiver with the receiving antenna index i and time index n , z_{in} represents the zero mean additive white Gaussian noise samples at the receiver, x_{jn} is the transmitted QAM constellation symbol with transmit antenna index j and h_{ij} is a zero mean, unit variance complex Gaussian channel gain (Rayleigh channel distribution) between the transmit antenna with index j and receive antenna with index i .

The performance of this scheme is shown in Fig. 3.7. ML-decoding was performed with a sphere decoder [57]. It can be observed that for a fixed constellation, the slope of the block error probability curve tends to 4 at high SNRs. Moreover the separation between the curves is approx 6dB at high SNRs, which indicates a multiplexing gain of 2b/s/Hz per dB, as expected from the tradeoff. While the 4-QAM curve is within 5dB of the outage probability curve, for higher constellations the gap reduces to less than a dB from the optimum. This gap can be further reduced by using outer error control coding, which gives a constant gain in SNR.

It is interesting to compare the performance of our random unitary modulation scheme with the rotated constellation based Yao-Wornell codes [61], [62]. Consider the unordered eigenvalue distribution of the Yao-Wornell dispersion matrix, in the 2×2 case, plotted in Fig. 3.8 alongside that of the 64-QAM with unitary dispersion. It is observed that while the smallest eigenvalue of the Yao-Wornell dispersion matrix

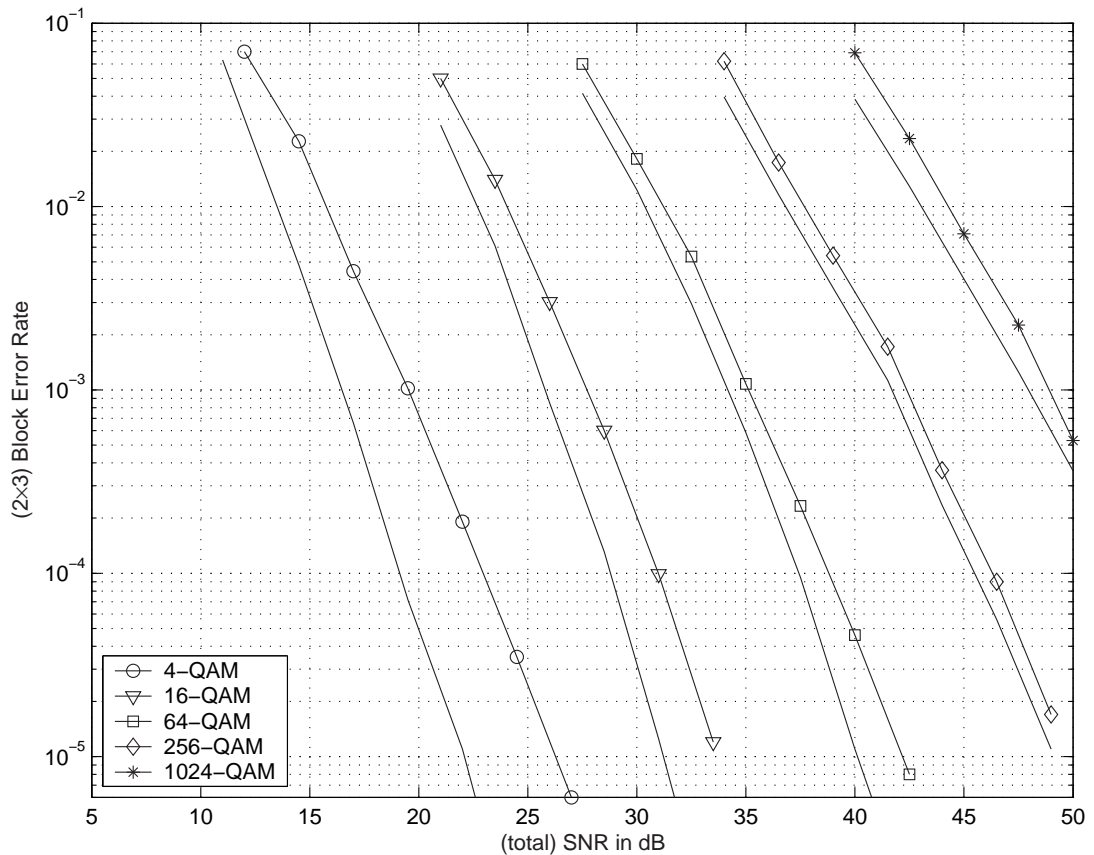


Figure 3.7: Block error rate(BER) with ML decoding(using a sphere decoder) for successive constellations with rates $R = 4, 8, 12, 16, 20$, alongside the corresponding outage probability curves.

is bounded away from zero, the distribution still peaks close to the origin (which reflects the asymptotic eigenvalue distribution for large arrays $\frac{1}{\pi}\sqrt{\frac{1}{\lambda} - \frac{1}{4}}$). On the other hand, even though the smallest singular values in the unitary dispersion case are comparable with the smallest singular value in the Yao-Wornell case, they are a smaller fraction of the total(the asymptotic eigenvalue distribution for large arrays has minimum eigenvalue $(1 - \sqrt{c})^2$). In fact, it can be observed from the plot that the singular value distribution peaks at considerable separation from the origin.

Finally, the choice of random unitary matrices is sufficient(as shown in [54]) to achieve the leftmost point(full diversity) on the diversity multiplexing tradeoff curve

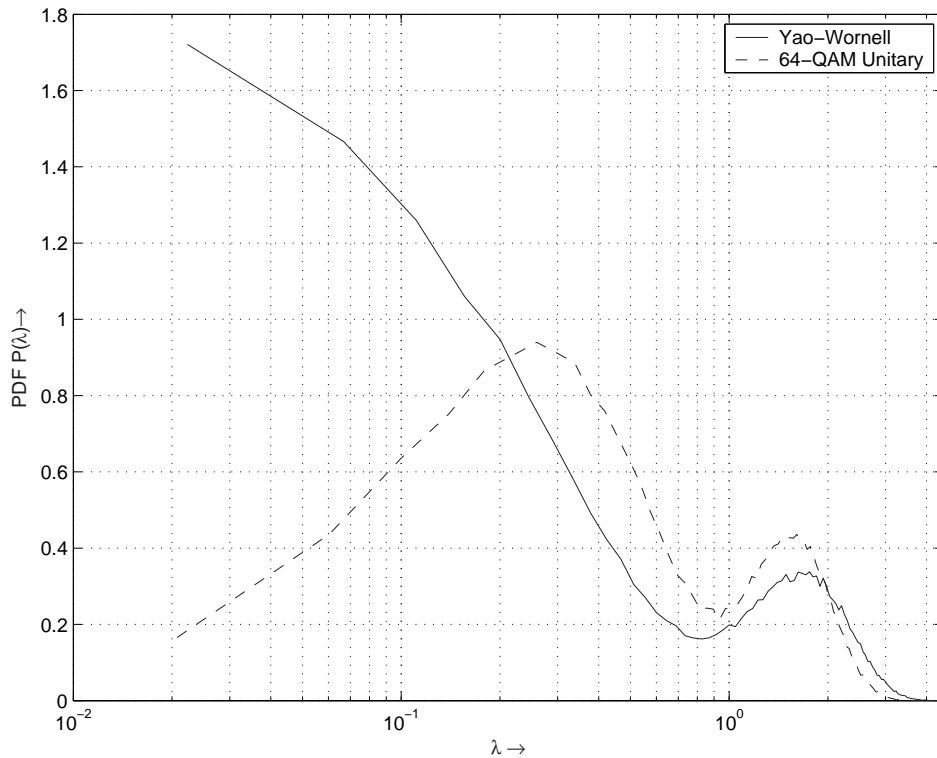


Figure 3.8: Probability density function (PDF) of the unordered eigenvalue λ of $\frac{1}{2}DD^*$ (where $D = X_i - X_j$ is the codeword difference matrix) for the Yao-Wornell codebook [61]. For the codebook obtained by unitary dispersion of the 64-QAM constellation, the eigenvalue λ corresponding to $\frac{1}{3}DD^*$ is plotted (the fraction $\frac{1}{3}$ normalises the power in each row to 1, in accordance with Silverstein’s limiting distribution theorem [42]). In both cases, the PDF is approximated by plotting the 100-bin histogram of 10^5 randomly generated 2×3 codeword matrices.

for any QAM symbol constellation. The random choice is also necessary, because well-known unitary matrices, such as the identity matrix or the FFT matrix, suffer a performance penalty in this case because all the codeword difference matrices are not full rank.

3.3 Conclusions

In the large array regime, we showed that it was possible to obtain the diversity multiplexing tradeoffs at finite SNRs, unlike the Zheng-Tse tradeoffs which are only valid in a limiting sense at high SNRs. However, for finite arrays, we obtained only a partial tradeoff curve for rates close to the ergodic mean rate. We showed that having equal or unequal antennas results in significantly different tradeoff behavior.

The limiting eigenvalue distribution of large arrays, which have minimum eigenvalue bounded away from zero, suggests that unitary linear dispersion with rectangular codeword blocks could achieve the full Zheng-Tse diversity multiplexing tradeoffs for finite antenna arrays. Our simulation results in the two-transmit, two-receive antennas case seem to confirm that full rate-full diversity designs (achieved by random unitary dispersion with probability one) gives us performance quite close to the outage probability bounds over an increasing sequence of constellations, which is necessary to achieve the full tradeoff.

Chapter 4

Impact of Vector Antennas on Range and Direction Estimation Using a Spherical Array

Multiple sensor arrays enable us to determine signal parameters with a much greater accuracy than single sensors. The use of multiple sensors for radar and sonar applications has been investigated for over three decades. A comprehensive summary of the first two decades can be found in [23].

One of the issues under investigation in recent years in radar [18, 28, 58], is on the benefit of using the polarization diversity of the electromagnetic medium for source localization. While an arbitrary EM field can have three degrees of freedom at every point in space, a plane EM wave is restricted to two, since it is constrained to have no field component in the direction of motion. With this restriction in mind, one can ask how much practical benefit there is in using an array of tri-polarized antennas versus an array of uni-polarized antennas(dipoles).

Multiple antennas sensors can be arranged in arrays of various shapes. Indeed,

a variety of array shapes have been investigated, implemented and deployed. While planar arrays are typically favored [39], recently there has been some interest in using spherical arrays [47]. The arguments cited by Tomasic et al. [47, 48], in favor of using a spherical array are: uniform beams in all directions, high gain, low mismatch and polarization losses, and 20% fewer radiating elements and transmit/recvie modules than other array configurations.

While practical arguments ultimately decide the choice between different shapes of antenna arrays, it is also of interest to compare the ultimate theoretical limits on parameter estimation for each array. The best estimate of a parameter is given by the maximum-likelihood/ML estimate. Even though the target parameter is fixed, in the presence of noise, the estimated parameter can never be exact and thus has a distribution of values. If the mean of the distribution matches the target parameter to be estimated, the parameter estimate is called 'unbiased'. In many typical examples, the ML estimate is unbiased. We may choose between different parameter estimates by comparing the variance of the distribution of the estimate. Interestingly, a universal lower bound on the variance of an unbiased parameter estimate is available, known as the Cramer-Rao Bound(abbreviated as CRB henceforth). However, the best possible estimate, which is the ML estimate, does not always achieve the Cramer-Rao lower bound. Still, it is commonly used as a benchmark to compare different parameter estimates. In many cases, the ML estimate achieves the CRB at high SNRs or some other asymptotic conditions.

Recently Dogandzic and Nehorai [9] investigated the fundamental CRB limits on range, velocity and direction estimation for spherical and other array structures composed of infinitesimal isotropic sensors uniformly distributed over the corresponding surface. However, their study assumed the incoming wave to be a scalar plane wave, with a single degree of freedom. In our more general study, we assume the incoming

wave is dual-polarized, having the full two degrees of freedom of a plane wave. We also take into account the effect of the antenna structure and orientation, instead of assuming an isotropic response. The goal of this work is to try and quantify this benefit more clearly for the special case of a spherical array of tripole antennas. Our criterion for the benefit from polarization corresponds to the accuracy with which a single source can be localized.

This chapter is organized as follows. In Sec. 4.1, we describe the assumptions in our system model. In Sec. 4.2 we determine the Cramer-Rao lower bound on the variance of range and direction estimates using a spherical array of tri-polarized and uni-polarized antennas. In Sec. 4.3 we discuss the choice of signals for and benefits from using vector antenna arrays and we summarize our results in Sec. 4.4.

4.1 Problem Formulation

We are interested in determining the location of a target located at $\{r, \theta, \phi\}$ in spherical co-ordinates, shown in Fig.4.1, centered at the receive array/source. The receiver is a spherical array/(shell) of (carrier-wavelength-normalized) radius R . The array is composed of infinitesimal antenna elements uniformly distributed over the surface of the sphere. The location of any antenna element on the surface of the receive array can be specified by spherical co-ordinates $\{R, \theta', \phi'\}$. Our goal is to estimate the parameter vector $\xi = [\xi_1, \xi_2, \xi_3]^T = [r, \theta, \phi]^T$ from the complex data collected from all the array elements.

We shall assume that the wave is traveling in a nonconductive, homogeneous and isotropic medium. The target will be assumed to be in the far-field, so the received

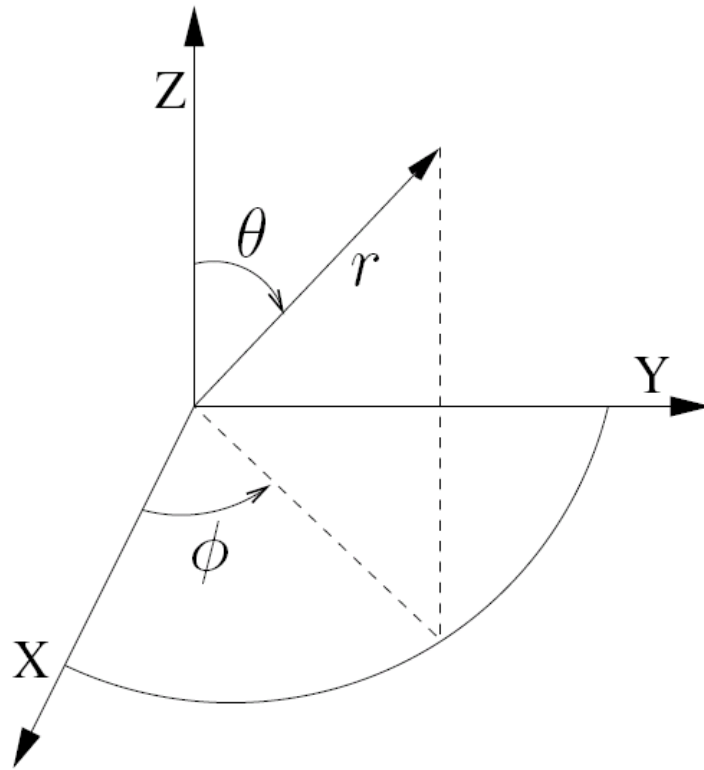


Figure 4.1: Spherical co-ordinate system with radius r , elevation angle θ and azimuth ϕ .

signal is a plane wave $E = [E_\theta, E_\phi]^T$, whose components can be written as

$$E_\theta(t) = s_1(t) \exp(j\omega_c t)$$

$$E_\phi(t) = s_2(t) \exp(j\omega_c t)$$

where ω_c is the carrier frequency in radians per second, and $\{s_1(t), s_2(t)\}$ complex numbers which represent the the amplitude and phase of the signal.

We shall assume the system is narrowband. This means that both the receive array and the target are of physically small dimensions compared to the signal wavelength. This is commonly referred to as the 'narrowband array assumption' [9], which implies that every array element can be assumed to receive the signal with the same delay for range estimation. In other words, this means that the range estimate which is

actually a time delay estimate, has negligible time spread and can just be treated as a single time delay estimate.

Each individual receiver output is amplified, converted to baseband(I and Q down-converters), low-pass filtered and sampled(I and Q samples), so the output is a complex phasor. We shall assume a coherent, equal energy ($\int_0^T |s_1(t)|^2 dt = \int_0^T |s_2(t)|^2 dt = 1$, without loss of generality since the signal amplitude can be absorbed into the noise variance σ^2 to maintain the same SNR) field which means in our model, after processing we get, $E_\theta(t) = s_1(t)$, $E_\phi(t) = s_2(t)$. For convenience, define the 2×1 vector signal $s(t) \equiv [s_1(t), s_2(t)]^T = E$.

The continuous time signal $s(t)$ is sampled at intervals Δt giving us samples $s(n\Delta t)$ for $n = 1, \dots, N$. Then the signal samples received by the array can be written as,

$$y(n\Delta t) = \mu(n\Delta t) + e(n\Delta t) = B_1(\boldsymbol{\theta}) \cdot s_1(n\Delta t - \tau) + B_2(\boldsymbol{\theta}) \cdot s_2(n\Delta t - \tau) + e(n\Delta t)$$

where μ is a $M \times 1$ noise free array response vector obtained by stacking the response of each of the M elements in the array, $\boldsymbol{\theta}$ is the vector of direction of arrival/DOA parameters $\{\theta, \phi\}$, $B_1(\boldsymbol{\theta})$ is the $M \times 1$ array response to the elevation component $E_\theta = s_1(n\Delta t - \tau)$, $B_2(\boldsymbol{\theta})$ is the $M \times 1$ array response to the azimuthal component $E_\phi = s_2(n\Delta t - \tau)$, $\tau = 2r/c$ is the total round trip time delay and e is a $M \times 1$ vector which represents the zero-mean, spatially and temporally correlated additive white Gaussian noise (AWGN).

Furthermore, stacking all the N time samples into a single vector, the system equation can be rewritten as,

$$\mathbf{y} = \boldsymbol{\mu}(\boldsymbol{\xi}) + \mathbf{e} = \mathbf{s}_1(\tau) \otimes B_1(\boldsymbol{\theta}) + \mathbf{s}_2(\tau) \otimes B_2(\boldsymbol{\theta}) + \mathbf{e}$$

where \otimes denotes the Kronecker product, and

$$\begin{aligned}\mathbf{y} &= [y(1\Delta t)^T, y(2\Delta t)^T, \dots, y(N\Delta t)^T]^T \\ \boldsymbol{\mu}(\xi) &= [\mu(1\Delta t, \xi)^T, \mu(2\Delta t, \xi)^T, \dots, \mu(N\Delta t, \xi)^T]^T \\ \mathbf{e} &= [e(1\Delta t)^T, e(2\Delta t)^T, \dots, e(N\Delta t)^T]^T \\ \mathbf{s}_i(\tau) &= [s_i(1\Delta t - \tau)^T, s_i(2\Delta t - \tau)^T, \dots, s_i(N\Delta t - \tau)^T]^T, \text{ for } i = 1, 2\end{aligned}$$

Assuming that the noise spatial and temporal covariances are separable, the noise spatio-temporal covariance matrix can be written as,

$$E[\mathbf{e}\mathbf{e}^*] = C \otimes \Sigma$$

where $(\cdot)^*$ denotes the conjugate transpose of a complex vector, C is the noise temporal covariance and Σ is the noise spatial covariance matrix.

4.2 Cramer-Rao Bounds

As we mentioned earlier, we wish to estimate the parameter vector $\xi = [\xi_1, \xi_2, \xi_3]^T = [r, \theta, \phi]^T$ from the complex data collected from all the array elements. It is well known that the maximum likelihood (ML) estimate is the best parameter estimate we can get. In the presence of complex additive white Gaussian noise (AWGN) with covariance matrix $\Omega(\xi)$, the conditional probability density function of the measurements is given by

$$p(y|\xi) = \frac{1}{\det(\pi\Omega(\xi))} \exp(-(y - \mu(\xi))^* \Omega^{-1}(\xi) (y - \mu(\xi)))$$

where $(\cdot)^*$ denotes the conjugate transpose of a complex vector. The ML estimate of ξ - written as $\hat{\xi}$ - is given by the maximum of $p(y|\xi)$ for a given y .

As we mentioned earlier, it is difficult to compute the distribution of the ML parameter estimate $\hat{\xi}$, but we can lower-bound its variance using the Cramer-Rao

bound/CRB which is a universal lower bound for any locally unbiased parameter estimate. To be more precise, if $C(\xi) = E\{(\xi - \hat{\xi})(\xi - \hat{\xi})^*\}$ is the covariance matrix of the estimation error, and $I^{-1}(\xi)$ (more on this shortly) is the CRB matrix, the difference matrix $C(\xi) - I^{-1}(\xi)$ is non-negative definite. The reason why we wrote the CRB matrix as $I^{-1}(\xi)$, is because it is obtained by inverting the Fisher information matrix/FIM, denoted by $I(\xi)$. The FIM $I(\xi)$ can be computed by taking the expectation of the Hessian of the conditional probability distribution,

$$[I(\xi)]_{ij} = E \left\{ \frac{\partial p(y|\xi)}{\partial \xi_i} \frac{\partial p(y|\xi)}{\partial \xi_j} \right\}$$

For the complex AWGN distribution specified above, the FIM $I(\xi)$ takes the following form [21, Appendix 15C],

$$[I(\xi)]_{ij} = Tr \left[\Omega^{-1}(\xi) \frac{\partial \Omega(\xi)}{\partial \xi_i} \Omega^{-1}(\xi) \frac{\partial \Omega(\xi)}{\partial \xi_j} \right] + 2Re \left[\frac{\partial \mu^*(\xi)}{\partial \xi_i} \Omega^{-1}(\xi) \frac{\partial \mu^*(\xi)}{\partial \xi_j} \right]$$

Since the signal is known, we have a conditional estimation problem [43] in which case, the 3×3 Fisher information matrix $I(\xi)$, with the noise covariance structure in our system model simplifies to,

$$[I(\xi)]_{ij} = 2Re \left\{ \frac{\partial \mu(\xi)^*}{\partial \xi_i} (C^{-1} \otimes \Sigma^{-1}) \frac{\partial \mu(\xi)}{\partial \xi_j} \right\}$$

4.2.1 Tri-polarized Spherical Array

Now we compute the Cramer-Rao bound/CRB on locational parameter estimation for a discrete array of infinitesimal tripole antennas uniformly distributed on the surface of a sphere.

Consider a spherical array of M infinitesimal tripoles all of which are oriented in conformity with the source cartesian co-ordinate axes. The signal and array are shown in Fig.4.2.

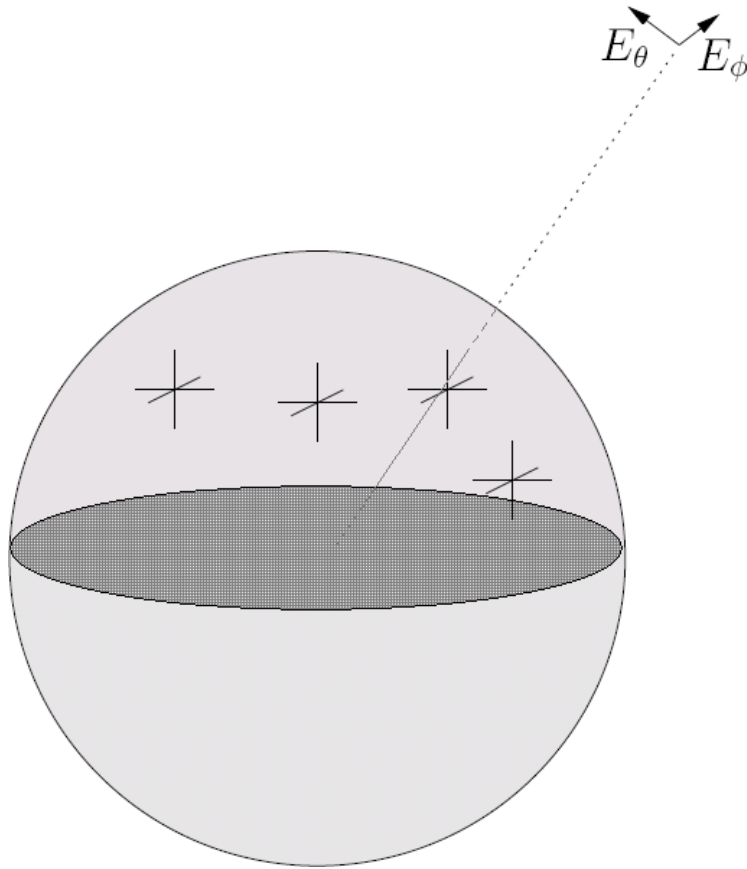


Figure 4.2: Spherical array with infinitesimal tripole antennas distributed uniformly on its surface, receiving a dual-polarized plane wave from a direction of arrival $\{\theta, \phi\}$.

The 3×1 response $\mu(t)$ of a tripole array element at a location $\{R', \theta', \phi'\}$ to the 2×1 far-field input $s(t - \tau) \equiv [s_1(t - \tau), s_2(t - \tau)]^T$, is given by

$$\begin{aligned} \mu(t) &= [B_1(\boldsymbol{\theta}) \ B_2(\boldsymbol{\theta})] e^{-j\alpha(\boldsymbol{\theta})} \begin{bmatrix} s_1(t - \tau) \\ s_2(t - \tau) \end{bmatrix} \\ &= \begin{bmatrix} s_1(t - \tau) \cos(\theta) \cos(\phi) - s_2(t - \tau) \sin(\phi) \\ s_1(t - \tau) \cos(\theta) \sin(\phi) + s_2(t - \tau) \cos(\phi) \\ -s_1(t - \tau) \sin(\theta) \end{bmatrix} e^{-j\alpha(\boldsymbol{\theta})} \end{aligned}$$

where $\alpha(\boldsymbol{\theta}) = 2\pi R(\sin(\theta) \sin(\theta') \cos(\phi - \phi') + \cos(\theta) \cos(\theta'))$.

Then, the FIM I_3 (the subscript indicates that it corresponds to the tri-polarized

case) is given by,

$$I_3 = 2Re \left\{ \frac{\partial \boldsymbol{\mu}(\boldsymbol{\xi})^*}{\partial \boldsymbol{\xi}} (C^{-1} \otimes \Sigma^{-1}) \frac{\partial \boldsymbol{\mu}(\boldsymbol{\xi})}{\partial \boldsymbol{\xi}^T} \right\}$$

which can be written as

$$I_3 = 2 \begin{bmatrix} I_{rr} & I_{\theta r}^T \\ I_{\theta r} & I_{\theta\theta} \end{bmatrix}$$

where

$$\begin{aligned} I_{rr} &= Re \left\{ \frac{\partial \mathbf{s}_1^*(\tau)}{\partial r} C^{-1} \frac{\partial \mathbf{s}_1(\tau)}{\partial r} \cdot B_1^*(\boldsymbol{\theta}) \Sigma^{-1} B_1(\boldsymbol{\theta}) + \frac{\partial \mathbf{s}_2^*(\tau)}{\partial r} C^{-1} \frac{\partial \mathbf{s}_2(\tau)}{\partial r} \cdot B_2^*(\boldsymbol{\theta}) \Sigma^{-1} B_2(\boldsymbol{\theta}) + \right. \\ &\quad \left. \frac{\partial \mathbf{s}_1^*(\tau)}{\partial r} C^{-1} \frac{\partial \mathbf{s}_2(\tau)}{\partial r} \cdot B_1^*(\boldsymbol{\theta}) \Sigma^{-1} B_2(\boldsymbol{\theta}) + \frac{\partial \mathbf{s}_2^*(\tau)}{\partial r} C^{-1} \frac{\partial \mathbf{s}_1(\tau)}{\partial r} \cdot B_2^*(\boldsymbol{\theta}) \Sigma^{-1} B_1(\boldsymbol{\theta}) \right\} \\ I_{\theta r}^T &= Re \left\{ \frac{\partial \mathbf{s}_1^*(\tau)}{\partial r} C^{-1} \mathbf{s}_1(\tau) \cdot B_1^*(\boldsymbol{\theta}) \Sigma^{-1} \frac{\partial B_1(\boldsymbol{\theta})}{\partial \boldsymbol{\theta}^T} + \frac{\partial \mathbf{s}_2^*(\tau)}{\partial r} C^{-1} \mathbf{s}_2(\tau) \cdot B_2^*(\boldsymbol{\theta}) \Sigma^{-1} \frac{\partial B_2(\boldsymbol{\theta})}{\partial \boldsymbol{\theta}^T} + \right. \\ &\quad \left. \frac{\partial \mathbf{s}_1^*(\tau)}{\partial r} C^{-1} \mathbf{s}_2(\tau) \cdot B_1^*(\boldsymbol{\theta}) \Sigma^{-1} \frac{\partial B_2(\boldsymbol{\theta})}{\partial \boldsymbol{\theta}^T} + \frac{\partial \mathbf{s}_2^*(\tau)}{\partial r} C^{-1} \mathbf{s}_1(\tau) \cdot B_2^*(\boldsymbol{\theta}) \Sigma^{-1} \frac{\partial B_1(\boldsymbol{\theta})}{\partial \boldsymbol{\theta}^T} \right\} \\ I_{\theta\theta} &= Re \left\{ \mathbf{s}_1^*(\tau) C^{-1} \mathbf{s}_1(\tau) \cdot \frac{\partial B_1^*(\boldsymbol{\theta})}{\partial \boldsymbol{\theta}} \Sigma^{-1} \frac{\partial B_1(\boldsymbol{\theta})}{\partial \boldsymbol{\theta}^T} + \mathbf{s}_2^*(\tau) C^{-1} \mathbf{s}_2(\tau) \cdot \frac{\partial B_2^*(\boldsymbol{\theta})}{\partial \boldsymbol{\theta}} \Sigma^{-1} \frac{\partial B_2(\boldsymbol{\theta})}{\partial \boldsymbol{\theta}^T} + \right. \\ &\quad \left. \mathbf{s}_1^*(\tau) C^{-1} \mathbf{s}_2(\tau) \cdot \frac{\partial B_1^*(\boldsymbol{\theta})}{\partial \boldsymbol{\theta}} \Sigma^{-1} \frac{\partial B_2(\boldsymbol{\theta})}{\partial \boldsymbol{\theta}^T} + \mathbf{s}_2^*(\tau) C^{-1} \mathbf{s}_1(\tau) \cdot \frac{\partial B_2^*(\boldsymbol{\theta})}{\partial \boldsymbol{\theta}} \Sigma^{-1} \frac{\partial B_1(\boldsymbol{\theta})}{\partial \boldsymbol{\theta}^T} \right\} \end{aligned}$$

For spatially and temporally white noise, i.e. $C = I, \Sigma = 1/\sigma^2 I$, where I is the identity matrix, σ^2 is the temporal noise variance for each antenna element, and for a spherical array, this yields the Fisher information matrix,

$$I_3 = \frac{M}{\pi \sigma^2} \begin{bmatrix} \frac{4}{c^2} \|\mathbf{s}'\|^2 & 0 & -\frac{2}{c} Re\{-\mathbf{s}_1'^* \mathbf{s}_2 + \mathbf{s}_2'^* \mathbf{s}_1\} \cos(\theta) \\ 0 & \|\mathbf{s}_1\|^2 + \|\mathbf{s}_2\|^2 \frac{8\pi R^2}{3} & Re\{\mathbf{s}_1^* \mathbf{s}_2\} \sin(\theta) \\ \frac{2}{c} Re\{\mathbf{s}_2^* \mathbf{s}_1' - \mathbf{s}_1^* \mathbf{s}_2'\} \cos(\theta) & Re\{\mathbf{s}_2^* \mathbf{s}_1\} \sin(\theta) & \|\mathbf{s}_1\|^2 \cos^2(\theta) + \|\mathbf{s}_2\|^2 + \frac{8\pi R^2 \|\mathbf{s}\|^2}{3} \sin^2(\theta) \end{bmatrix}$$

where the primes denote derivative w.r.t r , $\|\cdot\|$ denotes the norm of a vector (for example, $\|\mathbf{s}'\|^2 = \int_{-\infty}^{\infty} (|ds_1(\tau)/dr|^2 + |ds_2(\tau)/dr|^2) dt$, where $|\cdot|$ denotes the absolute value of a complex number) and we have dropped the arguments in $\mathbf{s}(\tau), \mathbf{s}_1(\tau), \mathbf{s}_2(\tau)$ for ease of presentation.

We observe that the entries of the FIM are independent of the azimuth ϕ . The Cramer-Rao bound matrix is given by $CRB_3(\boldsymbol{\xi}) = I_3^{-1}$.

4.2.2 Uni-polarized Spherical Array

Next, consider a spherical array of M infinitesimal uni-polarized antennas(dipoles) all of which are vertically oriented parallel to the z -axis. The 1×1 response of a uni-polarized array element to the input $s_1(t) = E_\theta(t)$ (the array has no response to the E_ϕ component) is given by

$$\mu(t) = -E_\theta(t) \sin(\theta) e^{-j\alpha} = s_1(t - \tau) B_1(\boldsymbol{\theta})$$

where $\alpha = 2\pi R(\sin(\theta) \sin(\theta') \cos(\phi - \phi') + \cos(\theta) \cos(\theta'))$.

Since the array responds to only one polarization component, the full system equation is given by,

$$\mathbf{y} = \boldsymbol{\mu}(\xi) + e = \mathbf{s}_1(\tau) \otimes B_1(\boldsymbol{\theta}) + e$$

Then, the FIM I_1 (the subscript indicates that it corresponds to the uni-polarized case) can be written as,

$$I_1 = 2 \begin{bmatrix} I_{rr} & I_{\boldsymbol{\theta}r}^T \\ I_{\boldsymbol{\theta}r} & I_{\boldsymbol{\theta}\boldsymbol{\theta}} \end{bmatrix}$$

where

$$\begin{aligned} I_{rr} &= \frac{\partial \mathbf{s}_1^*(\tau)}{\partial r} C^{-1} \frac{\partial \mathbf{s}_1(\tau)}{\partial r} \cdot B_1^*(\boldsymbol{\theta}) \Sigma^{-1} B_1(\boldsymbol{\theta}) \\ I_{\boldsymbol{\theta}r} &= \mathbf{s}_1^*(\tau) C^{-1} \frac{\partial \mathbf{s}_1(\tau)}{\partial r} \cdot \frac{\partial B_1^*(\boldsymbol{\theta})}{\partial \boldsymbol{\theta}} \Sigma^{-1} B_1(\boldsymbol{\theta}) \\ I_{\boldsymbol{\theta}\boldsymbol{\theta}} &= \mathbf{s}_1^*(\tau) C^{-1} \mathbf{s}_1(\tau) \cdot \frac{\partial B_1^*(\boldsymbol{\theta})}{\partial \boldsymbol{\theta}} \Sigma^{-1} \frac{\partial B_1(\boldsymbol{\theta})}{\partial \boldsymbol{\theta}^T} \end{aligned}$$

In the spatially and temporally white noise case, and for a spherical array, the FIM is given by,

$$I_1 = \frac{M}{\pi\sigma^2} \begin{bmatrix} \frac{4}{c^2} \|\mathbf{s}'_1\|^2 \sin^2(\theta) & 0 & 0 \\ 0 & \|\mathbf{s}_1\|^2 (\cos^2(\theta) + \frac{8\pi}{3} R^2 \sin^2(\theta)) & 0 \\ 0 & 0 & \|\mathbf{s}_1\|^2 \frac{8\pi}{3} R^2 \sin^4(\theta) \end{bmatrix}$$

The Cramer-Rao bound matrix is given by $CRB_1(\xi) = I_1^{-1}$. Here we observe that the FIM entries are uncoupled, independent of the signal shape as well as its azimuthal direction ϕ .

4.3 Gain From Polarization

Our goal in this section is to compare the accuracy with which a source can be localized using the tri-polarized and uni-polarized arrays.

For any given radar array, since all three location coordinates are uncertain, we can only locate the target within a certain region(volume) up to a certain confidence. In [9], it was shown that Wald's test gives a linearized confidence region defined by an ellipsoid. Further, it was shown in [9], that the square of the volume of the confidence ellipsoid $V(\xi)$ is proportional to the determinant of the CRB matrix $V^2(\xi) \propto \det(CRB(\xi))$. Since $\det(CRB(\xi))$ in spherical co-ordinates does not have the right dimensions for a squared volume, the constant of proportionality also includes a dimensional constant which is the same for both arrays. In any case, since the gain is a dimensionless quantity, we can compare the estimates obtained by the two arrays by simply taking the ratio of the determinant of the corresponding CRB matrices in spherical co-ordinates.

Signal Design

In order to compute the determinant of the CRB matrix, we need to fix our choice of signal. We would also like to choose signals such that the confidence volume of location, and hence equivalently, the determinant of the CRB matrix is minimized. Hadamard's inequality [4, pp. 126-130] states that for a positive definite matrix $A = [a_{ij}]$, the determinant is less than the product of its diagonal elements $\det(A) \leq$

$\prod a_{ii}$, with equality if and only if A is diagonal. In the uni-polarized case, the FIM is diagonal as it is. So we only have to consider the tri-polarized case. Note that the FIM and hence the CRB matrix are both positive definite matrices. Since the determinant of the CRB matrix $\det(CRB_3(\xi)) = 1/\det(I_3)$, we can minimize $\det(CRB_3(\xi))$ by maximizing $\det(I_3)$.

Hence, in the tri-polarized case we would like to choose signals which make the off diagonal entries in the FIM to be zero: $Re\{-\mathbf{s}'_1 \mathbf{s}_2 + \mathbf{s}'_2 \mathbf{s}_1\} = 0$, $Re\{\mathbf{s}'_1 \mathbf{s}_2\} = 0$. If we choose our signals to be scalar multiples of each other $s_2(t) = a s_1(t)$, the first condition can be immediately ensured. Note that $|a| = 1$, since both signals are of equal energy. Further, if we choose a circularly polarized signal with $a = \sqrt{-1}$, the second constraint is also satisfied. It only remains to choose a signal pulse shape appropriate for range estimation.

A commonly used signal in radar applications is the rectangular chirp pulse [53, p.292],

$$p(t) = \frac{1}{\sqrt{T_0}} \exp \left[j\pi \frac{f_B}{T_0} \left(t - \frac{1}{2}T_0 \right)^2 \right] \cdot [u(t) - u(t - T_0)]$$

where T_0 is the pulse duration, f_B is the bandwidth of the chirp pulse and $u(t)$ is the unit step function at the origin. If the time-bandwidth product of the pulse is large, $T_0 f_B \gg 1$, the spectrum of the pulse approaches a rectangular distribution [9, Appendix C] and hence the norm of the derivative is well approximated by $\|dp(t)/dt\|^2 = \int_{-\infty}^{\infty} |dp(t)/dt|^2 dt = \pi^2 f_B^2 / 3$.

Spherical Array Cramer-Rao Bounds

In what follows, we deliberately choose $3M$ to be the number of antennas in the array to ensure that a uni-polarized array with $3M$ antennas and a tri-polarized array with M tripoles, both have the same number of antennas, so that both the arrays estimate the data with the same number of measurements. Choosing signals

$s_1(t) = p(t)$ and $s_2(t) = i \cdot p(t)$, where $i = \sqrt{-1}$, the FIM I_3 in the tri-polarized case becomes,

$$I_3 = \frac{3M}{\pi\sigma^2} \begin{bmatrix} \frac{8\pi^2 f_B^2}{3c^2} & 0 & 0 \\ 0 & 1 + \frac{16\pi R^2}{3} & 0 \\ 0 & 0 & \cos^2(\theta) + 1 + \frac{16\pi R^2}{3} \sin^2(\theta) \end{bmatrix}$$

on inverting which, we get the following Cramer-Rao lower bounds on the location estimates for the tri-polarized spherical array,

$$\begin{aligned} \text{var}(r) &\geq \frac{\sigma^2 c^2}{8M\pi f_B^2}, \\ \text{var}(\theta) &\geq \frac{\pi\sigma^2}{3M} \frac{1}{\left(1 + \frac{16\pi R^2}{3}\right)}, \\ \text{var}(\phi) &\geq \frac{\pi\sigma^2}{3M} \frac{1}{\left(\cos^2(\theta) + 1 + \frac{16\pi R^2}{3} \sin^2(\theta)\right)} \end{aligned}$$

To compare with the tripole case, for the uni-polarized array, we choose the same rectangular chirp pulse signal $s_1(t) = p(t)$, and we get the following bounds on the location estimates for the uni-polarized array,

$$\begin{aligned} \text{var}(r) &\geq \frac{\sigma^2 c^2}{4M\pi f_B^2}, \\ \text{var}(\theta) &\geq \frac{\pi\sigma^2}{3M} \frac{1}{\left(\cos^2(\theta) + \frac{8\pi R^2}{3} \sin^2(\theta)\right)}, \\ \text{var}(\phi) &\geq \frac{\sigma^2}{8MR^2} \frac{1}{\sin^4(\theta)} \end{aligned}$$

Polarization Gain

First, consider a signal received along the azimuthal plane of the co-ordinate system, i.e. $\theta = \pi/2$ and ϕ is arbitrary. The volume squared of the confidence

ellipsoid in the tri-polarized case is proportional to the determinant of the CRB matrix $V_3^2 \propto \det(CRB_3(\xi))$, which is simply given by multiplying the lower bounds on the variance of the parameter estimates,

$$V_3 \propto \sqrt{\frac{(\pi\sigma^2)^3 c^2}{72M^3 \pi^2 f_B^2} \frac{1}{\left(1 + \frac{16\pi R^2}{3}\right) \left(\cos^2(\theta) + 1 + \frac{16\pi R^2}{3} \sin^2(\theta)\right)}}$$

We observe that for large R ,

$$V_3 \propto \frac{\sigma^3 c}{16M f_B R^2} \sqrt{\frac{1}{8\pi M}}$$

Similarly, in the uni-polarized case, for large R , we get the confidence volume,

$$V_1 \propto \frac{\sigma^3 c}{8M f_B R^2} \sqrt{\frac{1}{4\pi M}}$$

As we discussed at the beginning of this section, the constant of proportionality is the same for both arrays, so the ratio $V_1/V_3 = 2\sqrt{2} = 2.83$, gives us the factor by which a large spherical tripole array can estimate the most likely volume of location of a source in the equatorial plane versus a spherical uni-polarized array. We formally define the gain as the ratio of the volumes of the confidence ellipsoids in the two cases, which will be used henceforth.

On the other hand, as $R \rightarrow 0$, the gain from using a vector array tends to ∞

$$\lim_{R \rightarrow 0} \frac{V_1}{V_3} = \lim_{R \rightarrow 0} \frac{\sigma^3 c}{8M f_B R^2} \sqrt{\frac{1}{4\pi M}} \frac{6M f_B}{\sigma^3 c} \sqrt{\frac{2M}{\pi}} = \lim_{R \rightarrow 0} \frac{3}{8R^2} \sqrt{\frac{2}{\pi}} \rightarrow \infty$$

This makes sense if we observe that as $R \rightarrow 0$, the spherical tripole array tends to a single infinitesimal tripole at the origin, whereas, the uni-polarized array tends to a single infinitesimal dipole antenna which is incapable of providing DOA information.

For elevations above or below the equatorial plane, as seen in Fig.4.3('same signal' curve legend), the gains from using a tripole array grow monotonically up to the poles(only θ in the range $\frac{\pi}{5} < \theta < \frac{\pi}{2}$ is shown for clarity), where the gain tends to

infinity, irrespective of array radius. It is easy to see why this happens, since a plane wave traveling vertically produces no response in a vertically oriented dipole antenna, i.e. the uni-polarized array is 'blind' to plane waves arriving in the direction of the poles.

Effect of Energy Constraints

So far we have compared the performance of the tri-polarized and uni-polarized arrays when both of them receive the same signal. But the uni-polarized array has no response to the azimuthal component of the incoming polarized wave at all. Suppose we constrain the received signal energy by both the arrays to be equal instead. This means the amplitude of the signal $s_1(t)$ in the uni-polarized array would have to be scaled by a factor of $\sqrt{2}$, so that it has the same energy as the two components of the polarized signal in the tripole array. This would halve all the lower bounds in the uni-polarized case. As a result, the volume of confidence region is scaled(reduced) by a factor of $2\sqrt{2}$ which results in a gain for a signal received in the equatorial plane to $V_1/V_3 = 1!$ So for large arrays, there is no gain from using either array in estimating the location of a signal in the equatorial plane in this case. This gain with the 'equal energy' constraint is also plotted in Fig.4.3. However, the gain still increases steeply as the source moves towards the poles, as before. It is seen that this additional power normalization scales down the gain uniformly(for large arrays) by a factor of $2\sqrt{2}$ at all elevation angles θ .

4.4 Conclusions

We have looked at the problem of locating the position of a target in free space using an array of infinitesimal antennas uniformly distributed on the surface of a

sphere which respond to both the polarization components of the reflected signal. We have shown that significant gains are possible from using vector antenna arrays instead of uni-polarized antenna arrays - we can expect a minimum factor-of- $2\sqrt{2}$ volume reduction, in the case of large arrays, in the location estimate of a source in the equatorial plane, when the same signal is received by the two arrays. However, in the large array case, when the arrays are constrained to receive signals with equal energy, there is no gain from using either array for a target located in the equatorial plane. But in either signal energy constraint scenario, the gain from using a tri-polarized array increases quite steeply as the target moves towards the poles.

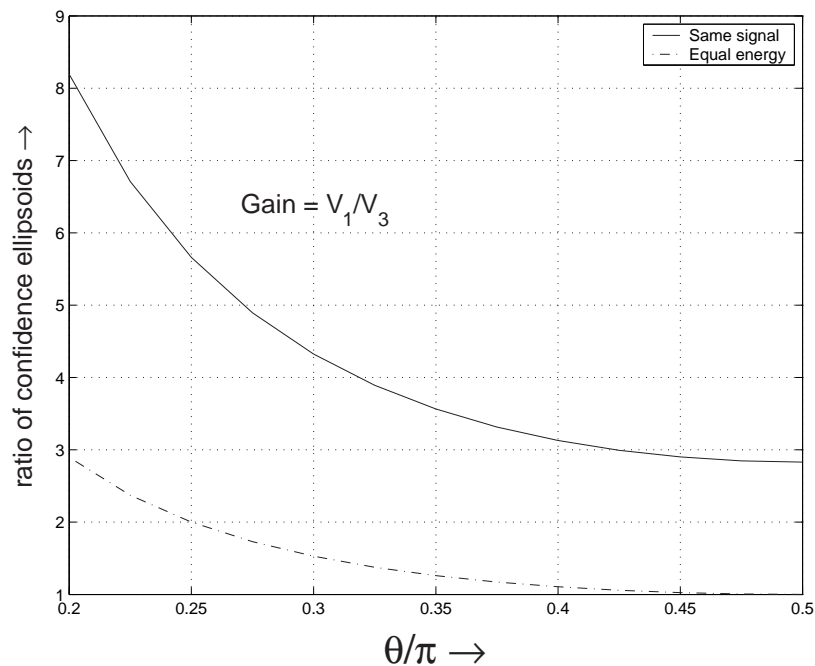


Figure 4.3: Ratio of confidence ellipsoid volume versus elevation angle, between an array of tri-polarized antennas and a uni-polarized antenna array. Both the arrays have a wavelength-normalized radius of $R = 10$, and the incoming wave is circularly polarized. The ticks on the x-axis mark the normalized elevation angle ($\frac{\theta}{\pi}$), for θ in the range $\frac{\pi}{5} < \theta < \frac{\pi}{2}$.

Chapter 5

Conclusions

In this dissertation, we have derived insights into the performance of multiple antenna systems in applications for communications and radar. We have derived asymptotically accurate formulae for large arrays, and shown that these can be used to approximate more easily the performance of finite array systems.

We first looked at the distribution of the mutual information in a point to point wireless link employing multiple antenna arrays at the transmitter and receiver. We showed, using recent results in random matrix theory, that this distribution tends to a Gaussian distribution in the limit, for large arrays, at all SNRs. We observed that in finite MIMO systems, the capacity distribution could be approximated closely by a Gaussian distribution and its mean and variance could be determined from the asymptotic limits which are given only in terms of the ratio of antennas in the transmit and receive arrays. In particular, the ergodic and outage capacities in finite MIMO arrays could be approximated closely using our asymptotic formulae. We discussed how the mean and variance of the distribution behave in the high and low SNR regimes.

We next applied our asymptotic capacity results to compute the diversity-multiplexing

tradeoff of large MIMO arrays in the finite SNR and high outage probability regime. We redefined the multiplexing and diversity gains suitably for application at finite SNR. We showed that symmetric and asymmetric arrays showed markedly different tradeoff behavior and discussed how this was a consequence of the limiting eigenvalue distribution of large arrays.

Using the insights obtained from the asymptotics, we showed by simulation that a full rate, full diversity random unitary matrix based linear dispersion coding scheme could achieve the full Zheng-Tse diversity multiplexing tradeoff. However, this requires the use of optimal ML decoding implemented by a sphere decoding algorithm. Schemes which could achieve the full tradeoff using a decoder of lower complexity remains an open problem.

Finally, we found Cramer-Rao lower bounds for variance of the location estimate of a target using a densely packed spherical array of infinitesimal uni-polarized and vector(tri-polarized) antennas. We found signals which minimized the confidence volume for the vector array. By taking the ratio of the confidence volumes of the uni-polarized array with the vector array, we obtained the gain from using polarization diversity. We discussed how the gain varies depending on the elevation and azimuth of the target, and also according to the energy constraint on the received signal.

Bibliography

- [1] S. M. Alamouti, “A Simple Transmit Diversity Technique for Wireless Communications,” *IEEE J. Select. Areas Commun.*, Vol. 16, No. 8, pp. 1451–1458, Oct. 1998.
- [2] Z. D. Bai and J. W. Silverstein, “CLT of linear spectral statistics of large dimensional sample covariance matrices” *Annals of Probability*, vol. 32, pp. 553-605, 2004.
- [3] Z. D. Bai and J. W. Silverstein, “No eigenvalues outside the support of the limiting spectral distribution of large dimensional random matrices,” *Annals of Probability* 26(1), pp. 316-345, 1998.
- [4] Bellman, R., “Introduction to Matrix Analysis,” 2nd ed. New York: McGraw-Hill, 1970.
- [5] C. Chuah, D. Tse, J. Kahn and R. Valenzuela, “Capacity scaling in MIMO wireless systems under correlated fading,” *IEEE Trans Inform Theory*, vol. 48, no. 3, pp. 637–650, March 2002.
- [6] Compton Jr., R., “The tripole antenna: An adaptive array with full polarization flexibility,” *IEEE trans. Antennas and Propagation*, vol. 29, pp. 944–952, Nov. 1981.

- [7] T. M. Cover, J. A. Thomas, “Elements of Information Theory,” *John Wiley and Sons, Inc.*, Canada, 1991.
- [8] Dayal, P. and Varanasi, M., “An optimal two transmit antenna space-time code and its stacked extensions” *Proceedings of Asilomar Conference on Signals, Systems and Computers*, CA, November 2003.
- [9] Dogandzic, A. and Nehorai, A., “CramerRao Bounds for Estimating Range, Velocity, and Direction with an Active Array,” *IEEE Transactions on Signal Processing*, vol. 49, no. 6, pp. 1122-1138, June 2001.
- [10] G. J. Foschini and M. J. Gans, “On limits of wireless communications in a fading environment when using multiple antennas,” *Wireless Personal Communications*, vol. 6, no. 3, pp. 311–335, March 1998.
- [11] G. J. Foschini, “Layered space-time architecture for wireless communication in a fading environment when using multi-element antennas,” *Bell Labs Tech. J.*, vol. 1, no. 2, pp. 4159, 1996.
- [12] G. Foschini, G. Golden, R. Valenzuela, and P. Wolniansky, “Simplified processing for high spectral efficiency wireless communication employing multi-element arrays,” *IEEE J. Select. Areas Commun.*, vol. 17, pp. 1841-1852, Nov. 1999.
- [13] R. G. Gallager, “Information Theory and Reliable Communications,” *John Wiley*, New York, 1968.
- [14] H. Ge, D. Wong, M. Barton and J. Liberti, “Statistical characterization of multiple-input multiple-output (MIMO) channel capacity”, *Proc. Wireless Networking Commun Conf (WCNC'02)*, pp. 789–793, Orlando, FL, Mar. 17–21, 2002.

- [15] G. D. Golden, C. J. Foschini, R. A. Valenzuela, P. W. Wolniansky, "Detection Algorithm and Initial Laboratory Results using V-BLAST Space-Time Communication Architecture," *IEEE Electronics Lett.*, Vol. 35, Issue 1, pp. 14-16, Jan. 1999.
- [16] B. Hassibi, and B.M. Hochwald, "High-rate codes that are linear in space and time," *IEEE Trans. Inform. Theory*, vol. 48, pp. 1804-1824, July 2002.
- [17] B. Hochwald, T. L. Marzetta, V. Tarokh, "Multi-Antenna Channel Hardening and its Implications for Rate Feedback and Scheduling," *IEEE Transactions on Information Theory*, vol 50, no. 9, pp. 1893 - 1909, Sept. 2004.
- [18] Hochwald, B. and Nehorai, A., "Polarimetric modeling and parameter estimation with applications to remote sensing," *IEEE Trans. Signal Processing*, vol. 43, pp. 1923-1935, Aug. 1995.
- [19] W. C. Jakes, "Microwave Mobile Communications," *Wiley*, 1974.
- [20] M.A. Kamath and B.L. Hughes, "The Asymptotic Capacity of Multiple-Antenna Rayleigh Fading Channels," *submitted to IEEE Trans. Inform. Theory*, 2002.(accepted)
- [21] Kay, S. M., "Fundamentals of Statistical Signal Processing: Estimation Theory", Englewood Cliffs, NJ: Prentice-Hall, 1993.
- [22] C. Kose and R. Wesel, "Universal space-time trellis codes," *IEEE Trans. Inform. Theory*, vol. 49, no. 10, pp. 2717-2727, Oct. 2003.
- [23] Krim, H. and Viberg, M., "Two decades of array signal processing: The parametric approach," *IEEE Signal Processing Mag.*, vol. 13, no. 4, pp.67-94, July 1996.

- [24] Krishnamurthy, S.H., Konanur, A., Lazzi, G. and Hughes, B.L., “On the Impact of Polarimetric Vector Antennas in Wireless Communications,” *2003 Conference on Information Sciences and Systems, The Johns Hopkins University*, March 12-14, 2003.
- [25] Krishnamurthy, S.H., Konanur, A., Lazzi, G. and Hughes, B.L., “Ultrawide-band vector antennas for sensing and positioning,” *2004 Asilomar Conference on Signals, Systems and Computers*, vol. 1, pp. 1237 - 1241, Nov. 7-10, 2004.
- [26] L. E. Larsen and J. H. Jacobi, Eds., “Medical Applications of Microwave Imaging,” *Piscataway, NJ: IEEE Press*, 1986.
- [27] V. A. Marcenko and L. A. Pastur, “Distribution of eigenvalues for some sets of random matrices” *Math USSR Sbornik*, Vol. 1, pp. 457-483, 1967.
- [28] Nehorai, A. and Paldi, E., “Vector-sensor array processing for electromagnetic source localization,” *IEEE Trans. on Signal Processing*, Vol. 42, pp. 376-398, Feb. 1994.
- [29] Oyman, O., Nabar, R.U., Bolcskei, H., and Paulraj, A.J., “Characterizing the statistical properties of mutual information in MIMO channels: insights into diversity-multiplexing tradeoff,” *Conference Record of the Thirty-Sixth Asilomar Conference on Signals, Systems and Computers*, vol.1, pp. 521–525, 2002.
- [30] A. J. Paulraj, and C. B. Papadias, “Space-time processing for wireless communications,” *IEEE Signal Processing Magazine*, vol. 14, pp. 49-83, Nov. 1997.
- [31] Poon, A., Brodersen, R. and Tse, D., “Degrees of Freedom in Multiple Antenna Channels: A Signal Space Approach”, *IEEE Transactions on Information Theory*, vol. 51, no. 2, pp. 523-536, Feb. 2005.

- [32] A. S. Y. Poon, D. N. C. Tse, and R. W. Brodersen, “Degrees of freedom in multiple-antenna channels: a signal space approach,” *IEEE Tran. Information Theory*, vol. 51, pp. 523-536, Feb. 2005.
- [33] J. G. Proakis, “Digital Communications,” 2nd ed., New York: McGraw-Hill, 1989.
- [34] G. G. Raleigh and J. M. Cioffi, “Spatio-temporal coding for wireless communication” *IEEE Transactions on Communications*, vol. 46, pp. 357-366, March 1998.
- [35] C. R. Rao, “Linear statistical inference and its applications,” *New York: Wiley*, 1973.
- [36] P. Rapajic and D. Popescu, “Information capacity of a random signature multiple-input multiple-output channel,” *IEEE Trans Commun*, vol. 48, no. 8, pp. 1245–1248, Aug. 2000.
- [37] T. S. Rappaport, “Wireless Communications, Principles and Practices,” *Prentice Hall*, Upper Saddle River, NJ, 1996.
- [38] Ravi Narasimhan, Amal Ekbal and John M. Cioffi, “Finite-SNR diversity-multiplexing tradeoff of space-time codes,” *Proc. IEEE International Conference on Communications (ICC 2005)* , 16 - 20 May 2005, Seoul, Korea.
- [39] Schuur, T. J., Zrnic, D. S., and Saffle, R. E. , “The Joint Polarization Experiment - An Overview of Initial Data Collection with a Polarimetric WSR-88D RADAR” *American Meteorological Society. 19th Conference on IIPS at the AMS Annual Meeting*, 9-13 Feb. 2003.

- [40] C. E. Shannon, "A Mathematical Theory of Communication," *The Bell System Technical Journal*, Vol. 27, pp. 379-423, Jul. 1948.
- [41] J. W. Silverstein, "The smallest eigenvalue of a large dimensional Wishart matrix," *Annals of Probability*, 13(4), pp. 1364-1368, 1985.
- [42] J. W. Silverstein, "Strong convergence of the empirical distribution of eigenvalues of large dimensional random matrices," *Journal of Multivariate Analysis*, vol. 55, no. 2, pp. 331-339, Nov. 1995.
- [43] Stoica, P. and Nehorai, A., "Performance Study of Conditional and Unconditional Direction-of-Arrival Estimation," *IEEE Transactions on Acoustics, Speech and Signal Processing*, vol. 38, no. 10, pp. 1783-1795, Oct. 1990.
- [44] V. Tarokh, N. Seshadri, and A. R. Calderbank, "Spacetime codes for high data rate wireless communication: Performance criterion and code construction," *IEEE Tran. Information Theory*, vol. 44, pp. 744-765, Mar. 1998.
- [45] S. Tavildar and P. Viswanath, "Approximately Universal Codes over Slow Fading Channels," to appear in *IEEE Transactions on Information Theory*, 2006.
- [46] I. E. Telatar, "Capacity of multi-antenna Gaussian channels," *European Transactions on Telecommunications*, vol. 10, no. 6, pp. 585-595, Nov. 1999.
- [47] Tomasic, B., Turtle, J., Shiang Liu, Schmier, R., Bharj, S. and Oleski, P., "The geodesic dome phased array antenna for satellite control and communication - subarray design, development and demonstration", *Phased Array Systems and Technology, 2003. IEEE International Symposium on*, pp. 411-416, Oct. 14-17, 2003.

- [48] Tomasic, B., Turtle, J. and Shiang Liu, "A Geodesic Sphere Phased-array Antenna for Satellite Control and Communication", *URSI GA 2002 - Oral and Poster Sessions*, Aug. 23, 2002.
- [49] D. Tse and P. Viswanath, "Fundamentals of Wireless Communication," Cambridge University Press, May 2005.
- [50] D. Tse, P. Viswanath and L. Zheng, "Diversity-Multiplexing tradeoff in multiple access channels", *IEEE Transactions on Information Theory*, Vol. 50(9), September 2004.
- [51] A. Tulino and S. Verdu, "Asymptotic Outage Capacity of Multiantenna Channels," *2005 IEEE Int. Conf. Acoustics, Speech and Signal Processing*, Philadelphia, PA, March 2005.
- [52] A. M. Tulino, S. Verdu, "Random Matrices and Wireless Communications," *Foundations and Trends in Communications and Information Theory*, Vol. 1, No. 1, Jun. 2004.
- [53] Van Trees, H. L., "Detection, Estimation and Modulation Theory. New York: Wiley," 1971, pt. III.
- [54] Varadarajan, B. and Barry, J.R., "Optimization of full-rate full-diversity linear space-time codes using the union bound", *Proceedings of the IEEE Information Theory Workshop*, pp. 210-213, March 31-April 4, 2003.
- [55] Varadarajan, B., "The Design of Linear Space-Time Codes For Quasi-Static Flat-Fading Channels", Ph.D. thesis, Georgia Institute of Technology, July 2004.

- [56] S. Verdú and S. Shamai (Shitz), “Spectral efficiency of CDMA with random spreading,” *IEEE Trans. Inform. Theory*, vol. 45, pp. 622–640, Mar. 1999.
- [57] H. Vikalo and B. Hassibi, “The expected complexity of sphere decoding, Part I: Theory, Part II: Applications,” *IEEE Trans. Signal Processing*, submitted for publication.
- [58] Weiss, A.J. and Friedlander, B., “Maximum Likelihood Signal Estimation for Polarization Sensitive Arrays,” *IEEE Transactions on Antennas and Propagation*, vol. 41, no. 7, July 1993.
- [59] J. Winters, “Smart Antennas for Wireless Systems,” *IEEE Pers. Commun.*, Feb. 1998, pp. 2327.
- [60] A. Wittneben, “A new bandwidth efficient transmit antenna modulation diversity scheme for linear digital modulation,” *Proc. 1993 IEEE International Conf. Communications (ICC93)*, pp. 16301634, May 1993.
- [61] H. Yao and G.W.Wornell, “Achieving the full MIMO diversity-vs-multiplexing frontier with rotation-based space-time codes,” in *Proc. 41th Annu. Allerton Conf. Communication, Control, and Computing, Monticello, IL*, Oct. 2003.
- [62] H. Yao, “Efficient signal, code, and receiver designs for MIMO communication systems,” Ph.D. thesis, Massachusetts Institute of Technology, Cambridge, MA, June 2003.
- [63] L. Zheng and D. Tse, “Diversity and Multiplexing: A Fundamental Tradeoff in Multiple Antenna Channels”, *IEEE Transactions on Information Theory*, vol. 49, no. 5, May 2003.

Appendix A

Asymptotic Variance Derivation

We now derive the formula for $\sigma^2(c, \rho)$ given in (2.13). Starting with (2.12), apply the change of variable

$$z(m) = -\frac{1}{m} + \frac{c}{1+m},$$

to obtain

$$\sigma^2 = -\frac{1}{4\pi} \int_{\mathcal{C}_2} \int_{\mathcal{C}_1} \frac{\ln(1 + \rho z(m_1)) \ln(1 + \rho z(m_2))}{(m_1 - m_2)^2} dm_1 dm_2$$

where the \mathcal{C}_1 and \mathcal{C}_2 can both be taken as positive, with \mathcal{C}_1 inside \mathcal{C}_2 . Since we can choose C_x and C_y in (2.13) to both cross the real axis in the intervals $(-1/\rho, 0)$ and $(b(c), \infty)$, we can choose \mathcal{C}_1 and \mathcal{C}_2 to both cross the real axis in the intervals $(m(-1/\rho), m(0-)) = (m(-1/\rho), \infty)$ and $(m(b(c)), m(\infty)) = (-(1 + \sqrt{c})^{-1}, 0)$, where $m(z)$ is given in (2.10) and

$$m(0-) = \lim_{x \rightarrow 0-} m(x), \quad m(\infty) = \lim_{x \rightarrow \infty} m(x).$$

We can rewrite the inner integral as

$$\begin{aligned}
& \frac{1}{2\pi j} \int_{\mathcal{C}_1} \frac{\ln(1 + \rho z(m_1))}{(m_1 - m_2)^2} dm_1 \\
&= \frac{1}{2\pi j} \int_{\mathcal{C}_1} \frac{\frac{\rho}{m^2} - \frac{c\rho}{(1+m)^2}}{\left[1 - \frac{\rho}{m} + \frac{c\rho}{1+m}\right]} \frac{1}{(m - m_2)} dm \\
&= \frac{\rho}{2\pi j} \int_{\mathcal{C}_1} \frac{(m+1)^2 - cm^2}{m(m+1)(m-m_2)(m-\lambda_+)(m-\lambda_-)} dm \\
&= \frac{\rho}{2\pi j} \int_{\mathcal{C}_1} \frac{(m+1)^2 - cm^2}{\lambda_+(m+1)(m-m_2)(m-\lambda_-)} \left[\frac{1}{m-\lambda_+} - \frac{1}{m} \right] dm
\end{aligned}$$

where

$$\begin{aligned}
\lambda_+ &= -\frac{1}{2}(1 - \rho + c\rho) + \frac{1}{2}\sqrt{(1 - \rho + c\rho)^2 + 4\rho} \\
\lambda_- &= -\frac{1}{2}(1 - \rho + c\rho) - \frac{1}{2}\sqrt{(1 - \rho + c\rho)^2 + 4\rho}
\end{aligned}$$

Observing that $\lambda_+ = m(-1/\rho)$, we see that \mathcal{C}_1 can be taken to enclose the poles at $m = \lambda_+, 0$ but not those at m_2, λ_- and -1 . Thus we have

$$\begin{aligned}
& \frac{1}{2\pi j} \int_{\mathcal{C}_1} \frac{\ln(1 + \rho z(m_1))}{(m_1 - m_2)^2} dm_1 \\
&= \frac{\rho((\lambda_+ + 1)^2 - c\lambda_+^2)}{\lambda_+(\lambda_+ + 1)(\lambda_+ - m_2)(\lambda_+ - \lambda_-)} - \frac{\rho}{\lambda_+(-m_2)(-\lambda_-)} \\
&= \frac{1}{m_2} - \frac{1}{m_2 - \lambda_+}
\end{aligned}$$

where the last step follows from $\lambda_+(\lambda_+ + 1) = \rho(1 - c)\lambda_+ + \rho$, $\lambda_- \lambda_+ = -\rho$.

The asymptotic variance can therefore be expressed as

$$\begin{aligned}
\sigma^2 &= \frac{1}{2\pi j} \int_{\mathcal{C}_2} \ln(1 + \rho z(m)) \left[\frac{1}{m} - \frac{1}{m - \lambda_+} \right] dm \\
&= \frac{1}{2\pi j} \int_{\mathcal{C}_2} \ln\left(\frac{m - \lambda_-}{m + 1}\right) \left[\frac{1}{m} - \frac{1}{m - \lambda_+} \right] dm \\
&\quad + \frac{1}{2\pi j} \int_{\mathcal{C}_2} \ln\left(\frac{m - \lambda_+}{m}\right) \left[\frac{1}{m} - \frac{1}{m - \lambda_+} \right] dm
\end{aligned}$$

where \mathcal{C}_2 encloses only the poles at 0 and λ_+ . The second integral vanishes, since it has antiderivative

$$\frac{1}{2} \left[\ln\left(\frac{m - \lambda_+}{m}\right) \right]^2$$

which is single-valued over the contour. The first integral yields

$$\begin{aligned}\sigma^2 &= \ln(-\lambda_-) - \ln\left(\frac{\lambda_+ - \lambda_-}{\lambda_+ + 1}\right) \\ &= \ln\left(\frac{\rho - \lambda_-}{\lambda_+ - \lambda_-}\right) = -\ln\left(1 - \frac{\rho - \lambda_+}{\rho - \lambda_-}\right).\end{aligned}$$

To prove (2.13), it only remains to observe that $\rho - \lambda_+ = \rho v(c, \rho)$ and $\rho - \lambda_- = \rho c/v(c, \rho)$.

Appendix B

Asymptotic Variance and Stieltjes Transform

In the following, we show that an explicit formula similar to Eq.2.13 for the variance can be given in terms of the Stieltjes Transform. This is applicable in the more general case when either the transmit or the receive arrays are correlated. Let

$$m_r(z) = \int \frac{1}{\lambda - z} dF_r(z)$$

Note that this integral is itself asymptotically Gaussian with mean $m(z)$. Moreover from [2], we know that $\hat{m}(z) = r[m_r(z) - m(z)]$ converges to a zero-mean Gaussian process with covariance

$$R_{\hat{m}}(x, y) = \frac{m'(x)m'(y)}{(m(x) - m(y))^2} - \frac{1}{(x - y)^2} . \quad (\text{B.1})$$

We begin by rewriting the capacity as a function of the inverse SNR $z = \rho^{-1}$:

$$\mu(\rho) = \eta(z) = \int_0^\infty \ln \left(1 + \frac{\lambda}{z} \right) dF(\lambda) , \quad z > 0 . \quad (\text{B.2})$$

Observe that

$$\eta'(z) = \int_0^\infty \frac{1}{\lambda + z} dF(\lambda) - \frac{1}{z} = -m(-z) - \frac{1}{z} .$$

Since $\lim_{z \rightarrow \infty} \eta(z) = 0$, we have

$$\eta(z) = - \int_z^\infty \eta'(\zeta) d\zeta = \int_z^\infty \left(\frac{1}{\zeta} + m(-\zeta) \right) d\zeta .$$

Letting $\eta_r(z)$ denote the capacity with respect to F_r , we know that

$$\begin{aligned} \hat{\eta}(z) &= r[\eta_r(z) - \eta(z)] = \int_z^\infty r [m_r(-\zeta) - m(-\zeta)] d\zeta \\ &= \int_z^\infty \hat{m}(-\zeta) d\zeta \end{aligned}$$

From which it follows that $\hat{\eta}(z)$ is $\mathcal{N}(0, \sigma^2)$ with

$$\begin{aligned} \sigma^2 &= \int_z^\infty \int_z^\infty R_{\hat{m}}(-x, -y) dx dy \\ &= \int_z^\infty \int_z^\infty \left[\frac{m'(-x)m'(-y)}{(m(-x) - m(-y))^2} - \frac{1}{(x - y)^2} \right] dx dy \end{aligned}$$

In order to evaluate this, we look at

$$\begin{aligned} &\int_{z_1}^\infty \int_{z_2}^\infty R_{\hat{m}}(-x, -y) dx dy \\ &= \int_{z_1}^\infty \int_{z_2}^\infty \left[\frac{m'(-x)m'(-y)}{(m(-x) - m(-y))^2} - \frac{1}{(x - y)^2} \right] dx dy \\ &= \int_{z_1}^\infty \left[\frac{m'(-y)}{(m(-x) - m(-y))} + \frac{1}{(x - y)} \right]_{z_2}^\infty dy \\ &= \int_{z_1}^\infty \left[\frac{-m'(-y)}{m(-y)} - \frac{m'(-y)}{(m(-z_1) - m(-y))} \right. \\ &\quad \left. - \frac{1}{(z_1 - y)} \right] dy \\ &= [\log(m(-y)) - \log(m(-z_1) - m(-y)) \\ &\quad + \log(z_1 - y)]_{z_1}^\infty \\ &= \log \left(\frac{(m(-z_1) - m(-z_2))}{(z_1 - z_2)m(-z_1)m(-z_2)} \right) \end{aligned}$$

In the limit as $z_1 \rightarrow z_2 = z$, we have

$$\log \left(\frac{(m(-z_1) - m(-z_2))}{(z_1 - z_2)m(-z_1)m(-z_2)} \right) \rightarrow \log \left[\frac{m'(-z)}{m^2(-z)} \right] = \sigma^2 \quad (\text{B.3})$$

Noting that $\mu(\rho) = \eta(1/\rho)$, we can write the variance in terms of the ergodic capacity as

$$\sigma^2 = \log \left[\frac{\rho^2 \mu''(\rho) - 1}{(\rho \mu'(\rho) - 1)^2} \right] \quad (\text{B.4})$$